Plant Cell Advance Publication. Published on September 21, 2020, doi:10.1105/tpc.20.00384

RESEARCH ARTICLE

Endocytosis of BRASSINOSTEROID INSENSITIVE1 is Partly Driven by a Canonical Tyrosine-based Motif

Derui Liu[1,2,6], Rahul Kumar[1,2,7], Lucas A. N. Claus[1,2], Alexander J. Johnson[3], Wei Siao[1,2] Isabelle Vanhoutte[1,2], Peng Wang[1,2], Kyle W. Bender[4,8], Klaas Yperman[1,2], Sara Martins[5], Xiuyang Zhao[1,2], Grégory Vert[5], Daniël Van Damme[1,2], Jiří Friml[3], Eugenia Russinova[1,2,*]

[1]Department of Plant Biotechnology and Bioinformatics, Ghent University, 9052 Ghent, Belgium.
[2]Center for Plant Systems Biology, VIB, 9052 Ghent, Belgium.
[3]Institute of Science and Technology Austria, 3400 Klosterneuburg, Austria.
[4]Department of Plant Biology, University of Illinois Urbana-Champaign, Urbana, IL 61801, USA.
[5]Plant Science Research Laboratory (LRSV), UMR5546 CNRS/Université Toulouse 3, 24 chemin de Borde Rouge, 31320 Auzeville Tolosane, France.
[6]Current address: Department of Plant Pathology and Microbiology and Institute for Plant Genomics and Biotechnology, Texas A&M University, College Station, TX 77843, USA.
[7]Current address: Department of Plant Sciences, University of Hyderabad, Hyderabad-500046, Telangana, India.
[8]Current address: Department of Molecular and Cellular Plant Physiology, University of Zürich, 8008 Zürich, Switzerland.
*Corresponding author: eurus@psb.vib-ugent.be

Short Title: Tyrosine motif-dependent endocytosis of BRI1

One Sentence Summary: Canonical tyrosine endocytic motifs are functional in plants and control the internalization of plasma membrane proteins by the clathrin adaptor complex AP-2.

The author responsible for distribution of materials integral to the findings presented in this article in accordance with the policy described in the Instructions for Authors (www.plantcell.org) is: Eugenia Russinova (eurus@psb.vib-ugent.be).

ABSTRACT

Clathrin-mediated endocytosis (CME) and its core endocytic machinery are evolutionarily conserved across all eukaryotes. In mammals, the heterotetrameric adaptor protein complex-2 (AP-2) sorts plasma membrane (PM) cargoes into vesicles via the recognition of motifs based on tyrosine or di-leucine in their cytoplasmic tails. However, in plants, very little is known about how PM proteins are sorted for CME and whether similar motifs are required. In *Arabidopsis thaliana*, the brassinosteroid (BR) receptor BR INSENSITIVE1 (BRI1) undergoes endocytosis, which depends on clathrin and AP-2. Here we demonstrate that BRI1 binds directly to the medium AP-2 subunit, AP2M. The cytoplasmic domain of BRI1 contains five putative canonical surface-exposed tyrosine-based endocytic motifs. The tyrosine-to-

phenylalanine substitution in Y_{898}KAI reduced BRI1 internalization without affecting its kinase activity. Consistently, plants carrying the $BRI1^{Y898F}$ mutation were hypersensitive to BRs. Our study demonstrates that AP-2-dependent internalization of PM proteins via the recognition of functional tyrosine motifs also operates in plants.

INTRODUCTION

In plants, plasma membrane (PM)-resident receptors are selectively internalized through endocytosis, which is crucial for signal termination (by targeting the receptors for degradation) (Irani et al., 2012; Di Rubbo et al., 2013; Martins et al., 2015; Zhou et al., 2018) or signal activation (Ortiz-Morea et al., 2016; Ma et al., 2020). Clathrin-mediated endocytosis (CME) is the most studied route for the internalization of PM proteins in plants (Reynolds et al., 2018). Clathrin-coated vesicles (CCVs) are the main carriers for endocytic cargoes. CCVs assemble at the PM and *trans*-Golgi network/early endosomes (TGN/EEs) in plant cells (Dhonukshe et al., 2007; Narasimhan et al., 2020). Although CME in plants displays some differences from that in yeast and mammals (Gadeyne et al., 2014; Narasimhan et al., 2020), plants contain homologs of many core endocytic proteins, including clathrin coats (Dhonukshe et al., 2007; Kitakura et al., 2011; Wang et al., 2013), adaptor proteins (Bashline et al., 2013; Di Rubbo et al., 2013; Fan et al., 2013; Kim et al., 2013; Yamaoka et al., 2013), dynamins (Konopka et al., 2008), and uncoating factors (Adamowski et al., 2018).

The heterotetrameric adaptor protein complex-2 (AP-2) of the CME pathway is conserved in plants (Bashline et al., 2013; Di Rubbo et al., 2013; Fan et al., 2013; Kim et al., 2013; Yamaoka et al., 2013), but its function is not well established. In mammals, AP-2 is involved in the formation of CCVs from the PM, and AP-2 deficiency leads to embryonic lethality in mice (Zizioli et al., 1999; Mitsunari et al., 2005). By contrast, AP-2 is partially required, but not essential, for CME in yeast and the nematode *Caenorhabditis elegans* (Gu et al., 2008; Weinberg and Drubin, 2012). Similarly, *Arabidopsis thaliana* with loss-of-function of single AP-2 subunits are viable but display defects in vegetative and floral organ development (Fan et al., 2013; Kim et al., 2013; Yamaoka et al., 2013), effector-triggered immunity (Hatsugai et al., 2016), growth under nutrient-deficient conditions (Yoshinari et al., 2019), and hormonal responses (Di Rubbo et al., 2013; Kim et al., 2013). In *Arabidopsis*, AP-2 is implicated in CME of several PM proteins, including the PIN-FORMED (PIN) auxin transporter (Fan et al., 2013; Kim et al., 2013), the brassinosteroid (BR) receptor BR

INSENSITIVE1 (BRI1) (Di Rubbo et al., 2013), the boron (B) transporter BOR1 (Yoshinari et al., 2019), and the boric acid channel NODULIN26-LIKE INTRINSIC PROTEIN5;1 (NIP5;1) (Wang et al., 2017). However, the mechanisms that govern the recruitment of these proteins into CCVs are unclear.

In mammalian cells, AP-2 recognizes cargoes destined for internalization by binding to specific motifs in these proteins (Bonifacino and Traub, 2003). Two major types of canonical motifs have been reported. The first type is the tyrosine motif, YXXΦ, where Y is tyrosine (Tyr), X is any amino acid, and Φ is a bulky hydrophobic residue [leucine (L), isoleucine (I), methionine (M), valine (V) or phenylalanine (F)], which is recognized and directly bound by the medium AP-2 subunit, AP2M (Ohno et al., 1995). The second type is the acidic di-leucine motif [DE]XXXL[LI], [aspartic (Asp, D) and glutamic (Glu, E) acids], which is recognized by the small AP-2 subunit, AP2S (Kelly et al., 2008). AP2M exhibits a preference for YXXΦ recognition compared with the medium subunits of AP-1, AP-3, and AP-4, which mediate different trafficking routes (Ohno et al., 1995). YXXΦ motifs are found in the cytoplasmic parts of several plant PM proteins (Geldner and Robatzek, 2008), but only a few have been studied functionally (Ron and Avni 2004; Li and Pan, 2017; Yamamoto et al., 2018). Several observations point towards the functionality of tyrosine motifs in plants. For example, the polarized targeting of the membrane-anchored endo-1,4-β-D-glucanase KORRIGAN is affected when a YXXΦ motif is mutated (Zuo et al., 2000). A tyrosine-to-alanine substitution in the Y_{933}XXΦ motif in the tomato (*Solanum lycopersicum*) receptor-like protein ethylene-inducing xylanase2 (LeEix2) abolishes its ability to induce hypersensitive responses (Ron and Avni 2004; Li and Pan, 2017). Furthermore, a conserved Y_{505}XXΦ motif in the cytoplasmic loop of PIN2 is required for its constitutive endocytosis (Kleine-Vehn et al., 2011). YXXΦ motifs were identified in the largest cytoplasmic loop of the BOR1 transporter; mutations in these motifs affected the polar localization and degradation of BOR1 (Takano et al., 2010; Yoshinari et al., 2012; Yoshinari et al., 2019).

Regardless of these observations, the binding of a cargo to AP2M in an YXXΦ motif-dependent manner, which is important for CME, has only been demonstrated for the *Agrobacterium*-derived virulence protein VirE2. The internalization of VirE2 and *Agrobacterium* infection are facilitated by this interaction (Li and Pan, 2017). Although the cytoplasmic loop of PIN1 bound to AP2M *in vitro*, and three YXXΦ motifs (Tyr-260, Tyr-328 and Tyr-394) were required for this binding, surprisingly, none of them were essential for PIN1 endocytosis and recycling *in planta* (Sancho-Andrés et al., 2016). In contrast to PIN1, neither the interaction between AP2M and BOR1 *in vivo* (Yoshinari et al., 2019) nor the

interaction between the C-terminal μ homology domain (MHD) of AP2M and the CELLULOSE SYNTHASE6 (CESA6) subunit of the cellulose synthase complex *in vitro* (Bashline et al., 2013) relied on specific endocytic motifs. Interestingly, canonical YXXΦ motifs were needed for the interaction of BOR1 with AP-3 and AP-4 (Yoshinari et al., 2019). Even though these examples hint at the possibility that cargoes are recognized by adaptor complexes, including AP-2, through their YXXΦ motifs, the underlying mechanisms of cargo recognition by AP-2 in plants remain largely elusive.

BRs are polyhydroxylated steroidal hormones that are essential for plant growth, development, and immunity (Nolan et al., 2020). BRs are perceived at the cell surface by the ectodomain of the PM-localized receptor BRI1 and its co-receptor BRI1-ASSOCIATED KINASE1 (BAK1). BR signals are conveyed from the cell surface to the nucleus through a sequential intracellular signaling cascade that activates the master transcription factors BRASSINAZOLE-RESISTANT1 (BZR1) and BRI1-EMS-SUPPRESSOR1 (BES1)/BZR2 (Nolan et al., 2020). The PM pool of BRI1 mainly controls BR signaling, and impaired endocytosis results in constitutive BR responses (Irani et al., 2012; Di Rubbo et al., 2013; Martins et al., 2015; Zhou et al., 2018). BRI1 undergoes AP-2-dependent CME (Di Rubbo et al., 2013), but it is unclear how AP-2 recognizes BRI1. Here, we demonstrate that AP2M directly binds to the Y_{898}KAI motif present in BRI1. Mutations of this motif resulted in plants that accumulated BRI1 in the PM and were hypersensitive to BRs. Our study demonstrates that canonical tyrosine motifs are functional in plants and that they control the internalization of PM proteins by AP-2.

RESULTS

BRI1 Binds Directly to the AP2M Subunit

We previously showed that BRI1 co-localizes and co-immunoprecipitates with clathrin heavy chain (CHC) and AP-2 *in vivo* and that the endocytosis of BRI1 is compromised when the function of AP-2 is impaired (Di Rubbo et al., 2013). To further corroborate these findings, we evaluated the dynamic localization of BRI1 and AP-2 in the PM of *Arabidopsis* epidermal root cells of *bri1-116* seedlings expressing BRI1-GFP and AP2A1-mTagRFP. We examined the temporal behavior of the two proteins by dual-color Total Internal Reflection Fluorescence Microscopy (TIRFM) imaging (Dhonukshe et al., 2007; Johnson and Vert, 2017) (Figure 1A). Discrete foci of BRI1-GFP and AP2A1-mTagRFP were tracked and analyzed. We found that a proportion of BRI1-GFP colocalized with AP2A1-mTagRFP foci (32.4% ±

10.3 of BRI1 colocalized with AP2A1) and that they appeared to display similar dynamics and disappeared from the PM together (Figure 1B). To examine this further, we conducted a 'departure assay' (Johnson and Vert, 2017), where the BRI1-GFP tracks were aligned to the moments of their co-localizing AP2A1 track departure. This assay showed that BRI1 has a similar profile to AP2A1 in the PM and that a fraction of BRI1 co-internalizes with AP2A1 (Figure 1C). The association of BRI1 with AP-2 was confirmed by fractionation analyses of CCVs isolated from 7-day-old *bri1* seedlings expressing BRI1-mCitrine, in which BRI1 co-fractionated with CHC and AP2A (Figure 1D).

To visualize the association between BRI1 and AP-2 in living cells, we performed a ratiometric bimolecular fluorescence complementation (rBiFC) assay (Grefen and Blatt, 2012) in *Nicotiana benthamiana* leaf epidermal cells (Figure 1E). A combination between the C-terminally tagged BRI1 (fused with the C-terminal fragment of YFP, designated cYFP) and the C-terminally tagged PM-associated BRI1-interacting protein BR-SIGNALING KINASE1 (BSK1) (fused with the N-terminal fragment of YFP, designated nYFP) (Tang et al., 2008) was used as a positive control. The interaction between BRI1-cYFP and the PM-localized pattern recognition receptor PEP RECEPTOR1 (PEPR1)-nYFP (Ortiz-Morea et al., 2016) was used as a negative control. BRI1 interacted predominantly with AP2M, AP2S, and AP2A1, whereas its interaction with the AP1/2B1 subunit was always weaker (Figure 1E).

To establish whether BRI1 interacts directly with the AP2M subunit, we carried out *in vitro* glutathione S-transferase (GST) pull-down assays using the bacterially expressed MBP-tagged BRI1-cytoplasmic domain (CD) and the GST-tagged AP2M subunit. MBP-tagged BRI1-CD was pulled down by GST-AP2M (Figure 1F). Although GST or GST-fused proteins interacted non-specifically with free MBP or with MBP-fused proteins, the interaction between GST-AP2M and the free MBP was reduced by competition with BRI1-CD (Figure 1F), thus demonstrating a preference for, as well as a direct interaction between AP2M and BRI1-CD *in vitro*. Altogether, our data indicate that BRI1 associates directly with AP-2 through the AP2M subunit.

BRI1 Contains Canonical Tyrosine-based YXXΦ Endocytic Motifs

In mammals, the selection of PM proteins for internalization depends on the recognition of endocytic signals in their CDs by AP-2 (Ohno et al., 1995; Bonifacino and Traub, 2003; Kelly et al., 2008). As BRI1 interacted with AP2M, we explored whether putative YXXΦ motifs might reside in the intracellular part of BRI1. Six canonical YXXΦ motifs in the kinase domain of BRI1 were identified, including Y_{898}KAI, Y_{945}CKV, Y_{956}EFM, Y_{961}GSL, Y_{1058}QSF, and

Y_{1072}GVV (Figure 2A). All YXXΦ motifs except Y_{1072}GVV are surface-exposed (Bojar et al., 2014) (Supplemental Figure 1), making them plausible candidates for being recognized by AP-2.

BRI1 is a dual-specificity kinase that autophosphorylates on tyrosine: both Tyr-956 and Tyr-1072 are autophosphorylated residues (Oh et al., 2009a, 2009b). Phosphorylated tyrosine will likely not bind AP2M, as the hydrogen bond formed between the hydroxyl group of the tyrosine in the YXXΦ motif and the negatively charged Asp-176 in human AP2M, corresponding to the conserved Asp-183 in the *Arabidopsis* AP2M (Supplemental Figure 2), is vital for cargo recognition, owing to electrostatic repulsion (De Franceschi et al., 2016). Therefore, Y_{956}EFM and Y_{1072}GVV were not considered to be endocytic motifs, but Y_{956}EFM was used in this study as a negative control.

We wanted to determine whether any of the four remaining putative YXXΦ motifs (Y_{898}KAI, Y_{945}CKV, Y_{961}GSL, and Y_{1058}QSF) are also required for receptor activation. We therefore examined whether the substitution of each tyrosine residue with phenylalanine, alanine, serine, or the phosphomimetic glutamic acid would affect the kinase activity of BRI1 *in vitro* (Figure 2B-C, Supplemental Figure 3). The mutated BRI1-CD recombinant proteins were compared with the wild type (MBP-BRI1-CD) for their ability to autophosphorylate and to transphosphorylate the inactive kinase domain of the co-receptor $BAK1^{D416N}$ (GST-mBAK1-CD) (Wang et al., 2008). The catalytically inactive kinase $BRI1^{K911E}$ (MBP-mBRI1-CD) (Wang et al., 2005) was included as a negative control in both experiments. Commercial anti-phosphotyrosine (anti-pY), anti-phosphothreonine (anti-pT), and phosphospecific antibodies against BRI1-pS_{858}, BRI1-pS_{981}, BRI1-pT_{872}, BRI1-pY_{831} and BRI1-pY_{956} (Oh et al., 2009a) were used. Tyrosine to phenylalanine substitutions at positions Tyr-898, Tyr-961, and Tyr-1058 in BRI1 neither reduced its autophosphorylation (Figure 2B) nor affected the transphosphorylation on mBAK1 (Figure 2C). By contrast, the $BRI1^{Y945F}$ mutant displayed reduced autophosphorylation and transphosphorylation activities, while, as previously stated (Bojar et al., 2014), the $BRI1^{Y956F}$ mutant remained kinase inactive (Figure 2B-C). Interestingly, except for the $BRI1^{Y945S}$ mutant, substitution of the tyrosine with either alanine, serine, or glutamic acid abolished the kinase activity of BRI1 (Supplemental Figure 3), likely because of conformational changes in the kinase. These data suggest that Tyr-945 is required for BRI1 activation and it is not an endocytic motif, whereas Y_{898}KAI, Y_{961}GSL, and Y_{1058}QSF remained putative YXXΦ motifs.

The $BRI1^{Y898F}$ Mutant Is Hypersensitive to BRs

To examine the functionality of the putative BRI1 YXXΦ endocytic motifs *in vivo*, we generated full-length BRI1 carrying the individual Y898F, Y945F, Y956F, Y961F, or Y1058F mutations, C-terminally tagged the mutant proteins with mCitrine, and expressed them in the *bri1* null allele (Jaillais et al., 2011) driven by the native promoter. We assessed the expression of each transgene (Supplemental Figure 4) and selected at least two independent transgenic lines with expression levels comparable to those of the wild type BRI1-mCitrine (Martins et al., 2015; Zhou et al., 2018) for further analysis. The BRI1^{Y898F}, BRI1^{Y961F}, and BRI1^{Y1058F} mutants complemented *bri1* (Figure 3A). Interestingly, although the BRI1^{Y956F} mutant is kinase-impaired (Figure 2B-C), it partially complemented the *bri1* phenotype, whereas the kinase-dead BRI1^{K911E} did not (Figure 3A, Supplemental Figure 5A). Similarly, transgenic lines expressing the BRI1^{Y898S} and BRI1^{Y956S} mutants (with abolished BRI1 kinase activity *in vitro*; Supplemental Figure 3) complemented *bri1* only to some extent (Supplemental Figure 5A-B).

To estimate the effects of the Y898F, Y945F, Y956F, Y961F, and Y1058F mutations on BRI1 phosphorylation *in vivo*, we immunoprecipitated BRI1 from a microsomal fraction isolated from 6-day-old transgenic plants, followed by immunoblot analysis with anti-pT antibodies (Supplemental Figure 6). Whereas the phosphorylation of BRI1^{Y956F} was notably lower than that of the wild type BRI1, the phosphorylation of BRI1^{Y945F} was only slightly reduced, and that of BRI1^{Y961F}, BRI1^{Y1058F}, and BRI1^{Y898F} was comparable (Supplemental Figure 6). As phosphorylation of BRI1 is a prerequisite for its ubiquitination and subsequent degradation (Martins et al., 2015; Zhou et al., 2018), we assessed the ubiquitination of BRI1 using anti-Ub antibodies. The ubiquitination of BRI1 was reduced in the BRI1^{Y945F} and BRI1^{Y956F} mutant lines, but that of BRI1^{Y898F}, BRI1^{Y961F} and BRI1^{Y1058F} was either unchanged or slightly increased (Supplemental Figure 6).

Next, we evaluated the BR responses of all transgenic lines by measuring the length of dark-grown hypocotyls in the presence of increasing concentrations of the most biologically active BR, brassinolide (BL) (Figure 3B). The BRI1^{Y956F} transgenic plants exhibited BR insensitivity at 5 to 50 nM BL, likely due to impaired BRI1 kinase activity. Similarly, the $Y_{898}S$ and $Y_{956}S$ mutations in BRI1 provoked resistance to BL (Supplemental Figure 5C). Of the two BRI1^{Y945F} lines, only one showed BR insensitivity at 5 to 50 nM. The BRI1^{Y898F} plants displayed hypersensitivity to BL, which was more pronounced at 50 nM BL, whereas surprisingly, the BRI1^{Y1058F} seedlings were resistant to BL. The $Y_{961}F$ mutation in BRI1 did not affect BR responses, except that one transgenic line was hypersensitive to 50 nM BL (Figure 3B).

The application of BRs induces dephosphorylation of the BES1 transcription factor, which is commonly used as a BR signaling activation readout (Yin et al., 2002). Consistent with the results of our hypocotyl growth assay, upon exogenous BL treatment, the accumulation of dephosphorylated BES1 was higher in BRI1^{Y898F} plants than the wild type, a difference observed even prior to treatment (Figure 3C). In agreement with the results of the BR growth assay, the BRI1^{Y956F} plants displayed BR insensitivity and reduced BES1 dephosphorylation, whereas in the BRI1^{Y945F} plants, the BES1 dephosphorylation levels significantly decreased only at 100 nM BL (Figure 3C). Similarly, after treatment with BL, the Y898S and Y956S mutations in BRI1 led to a decrease in dephosphorylated BES1 (Supplemental Figure 5D-E). The dephosphorylation level of BES1 in BRI1^{Y961F} plants remained like that of the wild type, but BRI1^{Y1058F} plants, which were insensitive to BR in the hypocotyl growth assay (Figure 3B), now displayed only a slight decrease in BES1 dephosphorylation at 10 nM BL (Figure 3C). In agreement with the finding that BR signaling occurs from the PM (Irani et al., 2012; Di Rubbo et al., 2013; Martins et al., 2015; Zhou et al., 2018), the weak constitutive BR responses observed in the BRI1^{Y898F} mutant support our hypothesis that Y_{898}KAI might be an endocytic motif.

The Y898F, Y945F, and Y956F Mutations in BRI1 Impair Its Endocytosis

Next, we examined whether the Y898F mutation in the putative endocytic Y_{898}KAI motif of BRI1 affects the amount of this receptor in the PM. The Y945F, Y956F, Y961F, and Y1058F BRI1 mutants were used as controls. Given that the PM pool of BRI1 is regulated by endocytosis, secretion, and recycling, we evaluated the root meristem cells of 5-day-old *bri1* seedlings that expressed the mCitrine-tagged mutant forms of BRI1 following treatment with 50 μM cycloheximide (CHX) for 1.5 h to inhibit *de novo* protein synthesis. By measuring the fluorescence intensity of BRI1 in the PM compared to that in the cytoplasm, we observed that the amount of BRI1-mCitrine significantly increased in plants carrying the Y_{898}F, Y_{945}F, and Y_{956}F mutations in BRI1 but did not significantly differ in the BRI1^{Y961F} and BRI1^{Y1058F} mutants compared to the control (Figure 4A-B).

In *Arabidopsis*, Brefeldin A (BFA) is used to visualize the internalization of different PM cargoes, as it inhibits exocytosis, leading to the accumulation of PM proteins in BFA bodies (Geldner et al., 2001). The accumulation of BRI1-mCitrine in BFA bodies decreased in the BRI1^{Y898F}, BRI1^{Y945F}, BRI1^{Y956F}, and BRI1^{Y961F} transgenic lines and did not change in the BRI1^{Y1058F} lines compared to the wild type (Figure 4C-D). Similarly, the BRI1^{Y898S} and BRI1^{Y956S} lines exhibited compromised internalization, as the relative BRI1-mCitrine signal

was increased in the PM and respectively decreased in the BFA bodies (Supplemental Figure 5F-G). Using kymographs obtained from spinning-disk movies (Gadeyne et al., 2014; Martins et al., 2015; Zhou et al., 2018), we measured the dwell time of BRI1-mCitrine-labelled foci in the PM in different mutants (Figure 4E). The average residence time of BRI1 in the PM of the control wild-type BRI1-mCitrine was 22.26 s. We observed small but significant increases in the lifetimes of the $BRI1^{Y898F}$, $BRI1^{Y945F}$, and $BRI1^{Y956F}$ mutants (26.01-30.78 s for different transgenic lines), indicating that the endocytosis of BRI1 is significantly impaired by Y898F, Y945F and Y956F mutations.

To rule out the possibility that the increase in BRI1-mCitrine fluorescence intensity at the PM in the $BRI1^{Y898F}$, $BRI1^{Y945F}$, and $BRI1^{Y956F}$ lines is due to recycling because targeting of BRI1 to the vacuole from the TGN/EE or other post-Golgi compartments is compromised by the Tyr mutations, we carried out BFA washout experiments after the combined application of BFA (50 μM) and CHX (50 μM) for 30 min. Epidermal cells of the root meristem were imaged after a washout with medium containing CHX for 30, 60, 90, and 120 min (Supplemental Figure 7A). Quantification of the percentage of epidermal cells with BFA bodies and the BFA body size (Supplemental Figure 7B-C) revealed no obvious differences between the transgenic lines, suggesting that the relocalization of BRI1-mCitrine from the BFA bodies to the PM was not affected in these lines. This was further corroborated by assessing the vacuolar accumulation of BRI1-mCit in Y898F, Y945F, Y956F, Y961F, and Y1058F BRI1 mutants when grown in darkness for 4h (Supplemental Figure 8A-B). As expected, the vacuolar accumulation of $BRI1^{Y898F}$, $BRI1^{Y945F}$, $BRI1^{Y956F}$, and $BRI1^{Y961F}$ was reduced, likely due to decreased internalization. Altogether, our data show that the endocytosis of BRI1 is compromised by either the $Y_{898}F$ mutation or by mutations that impair the kinase activity of BRI1.

The Y^{898}KAI Motif in BRI1 Binds to AP2M

Because $BRI1^{Y898F}$ conferred BR hypersensitivity without affecting the kinase activity of BRI1, and the $BRI1^{Y898F}$ mutant showed reduced internalization, we tested whether the Y_{898}KAI motif is recognized by AP2M. Since the AP2M MHD is involved in specific interactions with endocytic cargo proteins (Traub and Bonifacino, 2013), we carried out an *in vitro* peptide pull-down assay (Figure 5) with purified MHD of AP2M fused to GST (Supplemental Figure 9). A mutated AP2M-$MHD^{D183A;W424A}$ version that is presumably deficient in cargo binding (Yamaoka et al., 2013) was also included. The residues Asp-183 and Trp-424 in *Arabidopsis* AP2M are conserved with the Asp-176 and Trp-421 residues in

human AP2M (Supplemental Figure 2) and were previously shown to be important for the AP-2-cargo interaction mediated by the YxxΦ motif (Owen and Evans, 1998; Nesterov et al., 1999). The N-terminally biotinylated three tandem repeats of the DVYKAI peptide, designated peptide 1, and its two variants, DVAKAI (peptide 2) and DVAKAA (peptide 3), served as baits (Figure 5A). The interaction between AP2M-MHD and the DVYKAI was significantly decreased by the introduced mutations (Figure 5B-C). As expected, the AP2M-MHD$^{D183A;W424A}$ mutant displayed reduced binding to both the wild-type DVYKAI peptide and the DVAKAI and DVAKAA mutant variants (Figure 5B-C). Altogether, our data indicate that AP2M recognizes the Y^{898}KAI motif in BRI1 to facilitate CME.

DISCUSSION

AP-2 and Endocytosis of BRI1

Here we identified the canonical tyrosine-containing motif Y_{898}KAI in the CD of BRI1 and demonstrated its functional importance in BRI1 endocytosis. In mammalian systems, the link between AP-2 and PM proteins relies on the presence of short linear sorting motifs in their intracellular parts; the most common motif, YXXΦ, binds directly to AP2M (Bonifacino and Traub, 2003). Such YXXΦ motifs are also present in plant PM proteins (Geldner and Robatzek, 2008), but only a few have been directly linked to CME (Ron and Avni 2004; Li and Pan, 2017; Yamamoto et al., 2018). Five surface-exposed (Bojar et al., 2014) canonical YXXΦ endocytic motifs (Y_{898}KAI, Y_{945}CKV, Y_{956}EFM, Y_{961}GSL, and Y_{1058}QSF) are present in the CD of BRI1 (Oh et al., 2009a). The Tyr-898, Tyr-961, and Tyr-1058 of these motifs are not tyrosine phosphorylation sites (Oh et al., 2009a), as tyrosine-to-phenylalanine substitutions did not abolish the auto- and transphosphorylation activities of BRI1 and fully complemented the null *bri1* mutant. Notably, only the Y898F mutation caused BR hypersensitivity, which resulted from an increase in the PM pool of functional BRI1 due to compromised endocytosis. Similar phenotypes had previously been observed when BRI1 endocytosis is impaired by interference with either the CME machinery (Irani et al., 2012; Di Rubbo et al., 2013) or BRI1 ubiquitination (Martins et al., 2015; Zhou et al., 2018); in both cases, CME and the subsequent degradation of the BR receptor are prevented. In mammalian systems, the YXXΦ signals interact with the medium subunits of other AP complexes (Bonifacino and Traub, 2003). Also in plants, AP-3 and AP-4 function in the vacuolar sorting of different proteins via the recognition of YXXΦ motifs (Fuji et al., 2016; Yoshinari et al., 2019). Although BRI1

accumulates in the vacuole in mutants impaired in AP-3 function (Zwiewka et al., 2011), whether AP-3 and AP-4 play a role in BRI1 degradation through YXXΦ motifs is unclear.

Nonetheless, we noticed that the BR hypersensitivity phenotype caused by the Y898F mutation was relatively weak and that the internalization of BRI1, although reduced, was not completely abolished. Interestingly, the Y961F substitution did not affect the function of BRI1 or its endocytosis. However, some transgenic *bri1* lines expressing BRI1^{Y961F} tended to show slight BR hypersensitivity. Thus, the Y_{961}GSL motif might also contribute to CME of BRI1. Indeed, a few studies in mammalian systems showed that two canonical tyrosine-based sorting signals function cooperatively as AP-2-binding sites and that only mutations in both completely abolish CME of the PM cargoes (Böhm et al., 1997; Fong et al., 2013). Although the Y1058F mutation did not affect the kinase activity of BRI1, we observed some BR insensitivity in the complemented *bri1* transgenic lines, suggesting defective BR signaling. After careful inspection, we realized that these plants displayed phenotypes resembling those of the weak *bak1* mutants (Gou et al., 2012). Therefore, we speculate that this mutation might specifically affect the BRI1-BAK1 interaction, but further investigation is needed to support this assumption. Nevertheless, endocytosis of BRI1 was not impaired by the Y1058F mutation.

Whereas BRI1 endocytosis was completely abolished by impairing the clathrin function (Irani et al., 2012), disruption of either the YXXΦ motif in BRI1 or AP-2 function (Di Rubbo et al., 2013) failed to fully block BRI1 internalization, raising the question of whether the endocytic sorting of BRI1 depends entirely on AP-2. Similar to BRI1, the mammalian epidermal growth factor receptor (EGFR) interacted with the AP2M subunit (Sorkin and Carpenter, 1993), but its ligand-induced endocytosis was inhibited in clathrin-depleted, but not AP-2-depleted cells (Motley et al., 2003), suggesting that other adaptors might facilitate the uptake of EGFRs. In plants, in addition to AP-2, the heterooctameric TPLATE complex (TPC) functions as an important CME adaptor (Gadeyne et al., 2014). TPC subunits interact with clathrin and AP-2 and are necessary for their recruitment to the PM (Gadeyne et al., 2014; Bashline et al., 2015). Indeed, the endocytosis of BRI1 was fully blocked in TPC-depleted cells (Gadeyne et al., 2014), but it is still unclear whether TPC is required for the recruitment of specific cargoes by recognizing motifs that are distinct from that of AP-2 or whether it is an essential component of early CME initiation in plant cells. Taken together, our research suggests that AP-2 is not absolutely required for CME of BRI1.

BRI1 Kinase Activity and Endocytosis

The kinase activity of mammalian receptor tyrosine kinases (RTKs) is required for their ligand-induced CME (Lamaze and Schmid, 1995). Ligand-activated receptors undergo conformational changes that coincide with phosphorylation of their CDs and, simultaneously, the activated receptors can influence CME by altering the activity of other CME proteins (Ogiso et al., 2002). For example, the recruitment of the adaptor protein growth factor receptor-bound protein2 (Grb2) and the ubiquitin ligase Casitas B-lineage lymphoma (Cbl) was necessary and sufficient to induce CME of EGFR and the ligand-induced autophosphorylation of EGFR was requirement for their binding (Huang and Sorkin, 2005). Moreover, the ligand-activated EGFR phosphorylates the β2 subunit of AP-2 on tyrosine, which depends on the di-leucine motif in the EGFR carboxyl terminus (Huang et al., 2003). Although mutating this motif did not affect the endocytosis of EGFR, its targeting for degradation was disrupted (Huang et al., 2003). Ligand binding activates BRI1, leading to phosphorylation of its intracellular kinase (Wang et al., 2008). As expected, plants expressing the kinase-defective BRI1 mutants were insensitive to BRs, perhaps due to compromised BR signaling. Notably, all kinase-impaired tyrosine mutants of BRI1 showed significantly reduced endocytosis. However, it remains unexplored whether ligand-activated BRI1 phosphorylates any of the AP-2 subunits and as such plays a role in recruiting CME machinery to facilitate its endocytosis. Although BRI1 has no canonical di-leucine motifs in its CD, our experiments revealed that BRI1 can associate with the AP2A1 and AP2S subunits (Figure 1E, Supplemental Figure 10). Further studies combining phosphoproteomics might resolve these questions.

Ubiquitination of mammalian RTKs triggers CME (Hurley et al., 2006), which often depends on their activation through phosphorylation (Hunter, 2007; Lemmon and Schlessinger, 2010). BRI1 is K63 polyubiquitinated *in vivo*, and ubiquitination promotes its endocytosis and sorting for vacuolar degradation (Martins et al., 2015). A ubiquitination-compromised but kinase-active $BRI1^{25KR}$ mutant accumulates in the PM, and transgenic plants expressing the mutant protein display BR-hypersensitive phenotypes (Martins et al., 2015). Interestingly, endocytosis of $BRI1^{25KR}$ was not completely abolished, but significantly reduced, as observed in the kinase-impaired Y945F and Y956F BRI1 mutants. Notably, the ubiquitination of BRI1 *in vivo* was significantly reduced in the kinase-impaired Y945F and Y956F mutants. The ubiquitination of BRI1 depends on the U-box (PUB) E3 ubiquitin ligases PUB12 and PUB13, and the ligand-dependent activation of BRI1 promote its association with these enzymes through their phosphorylation, which is further required for BRI1 ubiquitination (Zhou et al., 2018). Therefore, the reduced kinase activity of BRI1 likely

impairs its internalization by affecting the efficiency of its ubiquitination. Whether ubiquitin can act as an endocytic signal for BRI1 is not yet known. However, an increasing amount data indicate that ubiquitin associates with a subset of clathrin adaptors in plants (Nagel et al., 2017; Moulinier-Anzola et al., 2020).

Mechanisms Controlling the Degradation versus Recycling of BRI1

BRI1 is the best-characterized receptor kinase in plants (Nolan et al., 2020). BRI1 endocytosis and trafficking have been extensively studied, but our understanding remains incomplete, albeit some progress has been made. BR-stimulated signaling was found to occur primarily at the PM, and the prevailing consensus is that the endocytosis of activated BRI1 functions as a means of signal attenuation (Kleine-Vehn et al., 2011; Irani et al., 2012; Di Rubbo et al., 2013; Martins et al., 2015). This view is supported by the finding that BR signaling is enhanced in mutants in which CME is prevented (Irani et al., 2012; Di Rubbo et al., 2013) or in cells expressing ubiquitination-compromised BRI1 mutant proteins (Martins et al., 2015; Zhou et al., 2018). BRI1 endocytosis is thought to be independent of ligands, because exogenous BRs did not affect BRI1 internalization, recycling, or degradation (Geldner et al., 2007; Russinova et al., 2007; Martin et al., 2015; Luo et al., 2015). Nevertheless, because on the one hand, BRI1 activation and phosphorylation are required for its internalization (Zhou et al., 2018) and on the other hand, AP-2 binding does not depend on BRI1 activation (Di Rubbo et al., 2013), we speculate that BRI1 undergoes a basal endocytosis, which is dependent on AP-2, and a ligand-induced endocytosis, which relies on BRI1 ubiquitination. It is likely that ubiquitinated BRI1 is sorted for degradation, whereas ligand-free BRI1 is recycled back to the PM, a model very similar to that recently proposed for the boron transporter BOR1 (Yoshinari et al., 2019). This assumption is supported by the prediction that, in contrast to mammalian systems, recycling of ligand-bound BRI1 probably does not occur, because the lack of the pH gradient in the TGN/EEs (Luo et al., 2015) does not allow for ligand dissociation. Without excluding the possibility that the activated and ubiquitinated BRI1 is endocytosed independently of clathrin under certain conditions, this model is in agreement with the observation that neither defects in AP-2 nor in BRI1 ubiquitination could fully abolish its internalization. Albeit plausible, this mechanism awaits further research and validation.

METHODS

Plant Material and Growth conditions

Arabidopsis thaliana accession Columbia 0 (Col-0) was used as the wild type. *pBRI1-BRI1-mCitrine* expressed in *bri1* (BRI1-mCittine;*bri1*) and the *bri1* null mutant (GABI_134E10) were described previously (Jaillais et al., 2011; Martins et al., 2015; Zhou et al., 2018). BRI1-GFP;*bri1-116;*AP2A1-mTagRFP was generated by crossing pRPS5A:AP2A1-mTagRFP/Col-0 (Di Rubbo et al., 2013) into pBRI1:BRI1-GFP;*bri1-116* and selected based on antibiotic resistance and fluorescent signals. For each construct, two to four independent mono-insertional lines that were homozygous for both *bri1* mutations and the transgene were selected in the T3 generation. The lines with BRI1 expression comparable to that in BRI1-mCitrine;*bri1* were used for further analysis. The *bri1* null mutant was genotyped with specific primers (Supplemental Data Set 1). For phenotypic analysis, plants were grown for 6 weeks in soil at 22°C, 58% relative humidity, and a 16-h light/8-h dark regime, under a standard light intensity (110 μmol m^{-2} sec^{-1}) for the day period using full-spectrum fluorescent light bulbs. The *Arabidopsis* seeds were surface-sterilized with chlorine gas and sown on plates with half-strength Murashige and Skoog medium (½MS) containing 0.5% (w/v) sucrose, 0.8% (w/v) agar, and 2.5 mM 2-(N-morpholino)ethanesulfonic acid (MES) (pH 5.7). After vernalization for 2 days at 4°C, the plates were transferred to the growth room and the seeds grown at 22°C under a 16-h/8-h light/dark cycle or in the dark after 4 h of light for different lengths of time, depending on the experiments. Plants were grown on plates for 6 days for the microsomal protein preparation, for 7 days for CCV isolation, and for 5 days for the BRI1 internalization, recycling, and transcript analyses. For the BFA washout experiments, seedlings were treated as previously described (Luo et al., 2015). For quantification of vacuole targeting of BRI1, plants were grown under constant light for 5 days and transferred to the dark for 4 h as previously described (Martins et al., 2015).

Generation of Constructs

Arabidopsis transgenic lines expressing the mutated BRI1 were generated using pDONRP1P2-BRI1 as a template to obtain BRI1 carrying Y-to-F substitutions at Y_{898}, Y_{945}, Y_{956}, Y_{961}, or Y_{1058F}, Y-to-S substitutions at Y_{898} or Y_{956}, or K-to-E substitution at K_{911} by site-directed mutagenesis with the primers listed in Supplemental Data Set 1. For the final destination vectors, three-fragment recombination systems were used with the destination vectors pB7m34GW or pK7m34GW (Karimi et al., 2007) and the entry vectors pDONRP4P1r-pBRI1, pDONR221-BRI1, or mutated BRI1 versions and pDONRP2rP3-mCitrine (Jaillais et al., 2011; Martins et al., 2015). The resulting constructs expressing BRI1

variants under the control of their own promoters were transformed into the heterozygous *bri1* null mutant by the floral dip method (Clough and Bent, 1998).

For the rBiFC experiments, the cDNAs of *BRI1*, *BSK1*, *AP2A1*, *AP1/2B1*, *AP2S*, *AP2M* and *PEPR1* were cloned into pDONR221-P3P2 and the cDNA of *BRI1* was cloned into pDONR221-P1P4. pDONR221-P1P4-BRI1 was recombined with pDONR221-P3P2-PEPR1, pDONR221-P3P2-BSK1, pDONR221-P3P2-AP2A1 (without the stop codon), pDONR221-P3P2-AP1/2B1 (without the stop codon), pDONR221-P3P2-AP2M (without the stop codon), pDONR221-P3P2-AP2S (without the stop codon) into pBiFC-2in1-CC to generate pBiFC-BRI1-nYFP+PEPR1-cYFP, pBiFC-BSK1-nYFP+BRI1-cYFP, pBiFC-AP2A1-nYFP+BRI1-cYFP, pBiFC-AP1/2B1-nYFP+BRI1-cYFP, pBiFC-AP2S-nYFP+BRI1-cYFP, pBiFC-AP2M-nYFP+BRI1-cYFP, respectively, whereas PDONR221-P3P2-AP2A1 (with the stop codon), pDONR221-P3P2-AP1/2B1 (with the stop codon), pDONR221-P3P2-AP2M (with the stop codon) and pDONR221-P3P2-AP2S (with the stop codon) were recombined with pDONR221-P1P4-BRI1 into pBiFC-2in1-NC to generate pBiFC-nYFP-AP2A1+BRI1-cYFP, pBIFC-nYFP-AP1/2B1+BRI1-cYFP, pBiFC-nYFP-AP2M+BRI1-cYFP and pBiFC-nYFP-AP2S+BRI1-cYFP, respectively.

The clones used for protein expression were made as follows: the cDNA encoding the CD of BRI1 was cloned into pDEST17 and into pGEX5x-3 to express MBP-BRI1-CD and GST-BRI1-CD, respectively. The cDNAs encoding the full-length AP2M (in pDONR221) (Di Rubbo et al., 2013), the full-length AP2S (in pDONR221) (Di Rubbo et al., 2013), the BAK1 CD, MHD of AP2M (amino acids 177 to 438), and the AP2A1 appendage domain (amino acids 733 to 971) were cloned into pGEX KG Gateway, pGEX6p-1, pGEX-5-1, pOPINJ (GST fusion) (Berrow et al., 2007), and pOPINM (MBP fusion) (Berrow et al., 2007) by Gateway or in-fusion cloning to express GST-AP2M, GST-AP2S, GST-mBAK1-CD, GST-AP2M-MHD, and MBP-AP2A1 appendage domain, respectively. pDEST17-BRI1-CD was used as a template to generate BRI1-CD carrying the Y-to-F, Y-to-S, Y-to-A, or Y-to-E substitutions at Y_{898}, Y_{945}, Y_{956}, Y_{961}, or Y_{1058F} and the K-to-E substitution at K_{911} by site-directed mutagenesis with the primers listed in Supplemental Data Set 1. GST-AP2M-MHD and MBP-AP2A1 appendage domain were cloned into pOPINJ and pOPINM, respectively, by in-fusion cloning (Takara Bio Inc.). pOPINJ is an Addgene plasmid # 26045; http://n2t.net/addgene:26045; RRID: Addgene_26045 and pOPINM is an Addgene plasmid # 26044; http://n2t.net/addgene:26044; RRID:Addgene_26044.

Chemical Treatments

MG-132 (Merck, 10 mM stock in dimethylsulfoxide [DMSO]), brassinazole (BRZ) (TCI Europe N.V., 20 mM stock in DMSO), BL (Wako Pure Chemical Industries, 10 mM stock in DMSO), BFA (Sigma-Aldrich, 50 mM stock in DMSO), and CHX (Merck, 50 mM stock in DMSO) were used at the concentrations indicated.

In vitro GST Pull-down Assay

Fusion proteins were generated from bacterial protein expression vectors in the *Escherichia coli* BL21 strain grown in Luria-Bertani (LB) medium supplemented with 0.1 mM isopropyl β-D-1-thiogalactopyranoside (IPTG) and induced for 16 h at 16°C. The GST and MBP fusion proteins were purified with glutathione Sepharose 4B GST-tagged protein purification resin (GE Healthcare) and amylose resin (New England Biolabs), respectively, according to the manufacturers' standard protocols. BRI1-CD was obtained by digesting GST-BRI1-CD with Factor Xa protease (New England Biolabs), followed by collection of the flow-through after the digest product had been loaded with glutathione Sepharose beads. All the purified proteins were dialyzed with a dialysis bag (Sigma-Aldrich) according to the manufacturer's protocol and concentrated with 10-kD (for GST and MBP) or 50-kD (for the other proteins) cut-off filters (Millipore). Approximately 10 μg of GST or GST-fused proteins as baits and MBP or MBP-fused proteins as preys were loaded to carry out pull-down assays using a Pierce™ GST Protein Interaction Pull-Down Kit (Thermo Scientific). Bound proteins were analyzed by immunoblotting using α-GST (GE Healthcare, 1:5,000), α-MBP (New England Biolabs, 1:3,000), or α-BRI1 (gift from Michael Hothorn, University of Geneva, 1;3,000) antibodies. Representative images are shown in Figure 1F, and full-scan blots are shown in Supplemental Figure 11.

CCV Purification

Seven-day-old BRI1-mCitrine;*bri1* seedlings were grown in ½MS. A 30 g sample was ground at 4°C and fractionated to purify CCVs as described previously (Mosesso et al., 2018). Samples collected during the purification and the final CCV fraction were analyzed by immunoblot analysis with antibodies against organelles and/or cellular compartments. The antibodies used were: horseradish peroxidase-coupled monoclonal α-GFP (Miltenyi Biotech, 1:2,500), α-CHC (Santa Cruz Biotechnologies, 1:5,000), α-AP2A (Kim et al., 2013) (1:2,000), α-H^+ATPase (Agrisera, 1:5,000), α-Cyt c (Agrisera, 1:5,000), α-V-ATPase (Agrisera,

1:5,000), α-Toc75 (Agrisera, 1:5,000), α-BiP (Agrisera, 1:2,000), and α-Sec21p (Agrisera, 1:5,000). The full-scan blots are shown in Supplemental Figure 11.

***In vitro* Peptide Pull-down Assay**

GST-AP2M-MHD and GST-AP2M-MHD$^{D183A;W424A}$ were expressed in BL21 with LB medium supplemented with 0.1 mM IPTG and induced at 16°C for 16 h. For GST-AP2M-MHD, the collected *E. coli* pellet was sonicated in extraction buffer (20 mM 4-(2-hydroxyethyl)-1-piperazineethanesulfonic acid [HEPES], pH 7.4, 300 mM NaCl, 3 mM dithiothreitol [DTT]) and 10 mM imidazole, further purified on an IMAC 16/10 column (GE Healthcare), and eluted with the same buffer supplemented with 500 mM imidazole. The eluate was concentrated with a 10-kD cut-off filter to 0.5 ml and injected on a Superdex 10/300 200pg (GE Healthcare) with the same buffer used for the lysis, but without imidazole. Fractions eluting between 12 and 15 ml were collected and used.

For GST-AP2M-MHD$^{D183A;W424A}$, the collected pellet was sonicated in extraction buffer (50 mM Tris-HCl, pH 7.5, 300 mM NaCl, 1 mM ethylenediaminetetra-acetic acid (EDTA), 1 mM DTT) and further purified with glutathione Sepharose 4B GST-tagged protein purification resin (GE Healthcare) according to the manufacturer's instructions.

N-terminally biotinylated peptides (100 µg, custom-made by GenScript) were incubated with 20 µL streptavidin beads (Pierce) prewashed with phosphate buffered saline (PBS) for 1 h. Afterwards, the beads were washed three times with 1 mL PBS. The peptide-bound beads were further incubated with 1 µg purified protein for 2 h at 4°C. Flow-throughs were collected for further analysis and the beads were washed three times with 1 mL PBS. The bound proteins were eluted by boiling the beads in loading buffer at 95°C for 10 min and were analyzed by immunoblotting using α-GST (GE Healthcare, 1:5,000). Representative images are shown in Figure 5B, and full-scan blots are shown in Supplemental Figure 11.

TIRFM and Image Analysis

Seven-day-old seedlings were prepared as described (Johnson and Vert, 2017), additionally fixing the coverslips on the microscopy slides with nail polish. Images were acquired with an Olympus IX83 inverted microscope equipped with a Cell^TIRF module and an Olympus 1.49 NA 100× Uapo objective. Time lapses were collected at 1 Hz for 5 min. Co-localization rates were determined using ComDet (https://github.com/ekatrukha/ComDet/wiki) in Fiji, in which a medium Z projection of the particle detection of the first 10 frames of a time lapse was used. An average co-localization rate was obtained by combining data from six cells from

independent roots. The 'departure assay' was conducted as described (Narasimhan et al., 2020), and the AP2A1 channel was set as the reference.

Confocal Microscopy and Image Analysis

For the rBiFC imaging, *Agrobacterium* strain C58 carrying the constructs of interest and a p19-harbouring strain were co-infiltrated into *N. benthamiana* leaf epidermal cells as described previously (Boruc et al., 2010). Multiple infiltrated leaves were observed with a Leica SP8 confocal microscope and a HC PL APO CS2 40× water corrected immersion objective (numerical aperture of 1.10) 2 days after infiltration. Images were captured at 488 nm and 561 nm laser excitation and 520-548 nm and 598-633 nm emission for YFP and RFP, respectively. Autofluorescence was removed by the gating technology. Images were converted to 8-bit in ImageJ for the YFP and RFP signal intensity measurements. The whole PM regions were selected and the averages of the 100 most intense pixels were used to calculate the YFP/RFP signal ratio.

To analyze BRI1 internalization, vacuole targeting, or recycling, *Arabidopsis* seedlings were imaged with a 60× water corrected immersion objective for BRI1 internalization and vacuole targeting or a 40× water corrected immersion objective for BRI1 recycling, (numerical aperture of 1.2, and 1.3, respectively) on an inverted confocal laser scanning microscope (FluoView1000; Olympus). The excitation/emission wavelengths used were 514 nm/530-600 nm for BRI1-mCitrine. Images were converted to 8-bit in ImageJ for BRI1-mCitrine fluorescence signal intensity measurements. Regions of interest (ROIs) were selected based on the PM or cytosol localization, and the relative PM BRI1-mCitrine fluorescent levels were evaluated as described previously for the analysis of BRI1 internalization and vacuole targeting (Luo et al., 2015; Martins et al., 2015; Luo and Russinova, 2017). BFA body size and the percentage of epidermal cells with BFA bodies were measured and calculated as described for BRI1 recycling analysis (Luo et al., 2015).

To analyze BRI1 residency time, hypocotyls from 5-day-old etiolated seedlings were imaged with a spinning disc ultraview microscope (Perkin Elmer) equipped with a 100× oil immersion objective. The excitation wavelength used was 515 nm provided by diode laser excitation controlled by Volocity software (Quorum Technologies), and emission light was collected with an ET525/50m emission filter (Chroma Technology Corp.). Time lapses were acquired for 3 min at 500-ms intervals, and images were captured with an EMCCD camera (Hamamatsu Photonics). Videos of three independent experiments were processed with

ImageJ software. Kymographs were generated with a line thickness of 3, and a walking average of 4 was applied for their analysis.

qRT-PCR

Total RNA was extracted from 5-day-old seedlings with an RNeasy kit (Qiagen). cDNA from RNA was synthesized with the ImProm-II™ Reverse Transcription System (Promega). qRT-PCRs were performed with SYBR green I Master kit (Roche) on a LightCycler 480 (Roche). The *BRI1* expression was normalized to that of *ACTIN4*. The cycling conditions were: 95°C, 10 min (pre-incubation); 95°C, 10 seconds, 60°C, 15 seconds, and 72°C, 15 seconds (45 cycles of amplification); 95°C, 1 second, and 65°C, 1 second (melting curve); 40°C, 10 seconds (cooling).

Immunoblot Analysis and Immunoprecipitation

For the *BRI1* expression assay, 5-day-old seedlings were homogenized in liquid nitrogen. Total proteins were extracted with a buffer containing 20 mM Tris-HCl, pH 7.5, 150 mM NaCl, 1% (w/v) sodium dodecyl sulfate (SDS), 100 mM DTT and EDTA-free protease inhibitor cocktail cOmplete (Roche). For blocking and antibody dilutions, 3% (w/v) bovine serum albumin (BSA) powder in 0.2% (v/v) Tween-20 containing Tris-buffered saline was used. For microsomal fraction isolation, 5-day-old seedlings were first treated with 3 μM of the BR biosynthesis inhibitor BRZ (Asami et al., 2000) for 24 h to deplete the endogenous BRs completely, then with 50 μM MG-132 for 5 h and the last hour together with 100 nM BL to boost the BR signaling. The samples were ground in liquid nitrogen and resuspended in ice-cold sucrose buffer (100 mM Tris [pH 7.5], 810 mM sucrose, 5% [v/v] glycerol, 10 mM EDTA [pH 8.0], 10 mM ethyleneglycoltetraacetic acid [EGTA, pH 8.0], 5 mM KCl, protease inhibitor [Sigma-Aldrich] and phosphatase inhibitor [Sigma-Aldrich]). Microsomes were pelleted from the homogenate as described (Abas et al., 2006). The pellet was resuspended in immunoprecipitation buffer (25 mM Tris, pH 7.5, 150 mM NaCl, 0.1% [w/v] SDS, protease inhibitor and phosphatase inhibitor). Immunoprecipitations were carried out on solubilized microsomal proteins with GFP-Trap-MA (Chromotek) according to the manufacturer's protocol. For protein detection, the following antibodies were used: monoclonal α-GFP horseradish peroxidase-coupled (Miltenyi Biotech, 1:5,000), monoclonal α-tubulin (Sigma-Aldrich, 1:10,000), α-ubiquitin (Ub) P4D1 (Millipore, 1:2,500), α-pT (Cell Signaling, 1:2,000) and α-BES1 (Yin et al., 2002) (1:4,000). Representative images are shown in the figures, and full-scan blots are shown in Supplemental Figure 11.

Graphical Illustrations

The structure of the BRI1 kinase domain (Bojar et al., 2014) was visualized, and the molecular graphics were generated and analyzed using UCSF Chimera (Pettersen et al., 2004), developed by the Resource for Biocomputing, Visualization, and Informatics at the University of California, San Francisco.

Quantification and statistical analysis

Statistical analyses were all done in Excel with build-in formulas. The *P* values were calculated with two-tailed Student's unpaired *t*-test analysis for binary comparison, or with one-way ANOVA and Tukey's post hoc honest significance test for comparisons of more than two genotypes. The measurements shown in box plots are displaying the first and third quartiles and are split by medians (center lines), with whiskers extending to 1.5-fold the interquartile range from the 25th and 75th percentiles. Outliers are represented by dots. Asterisks illustrate the *P* values: **, $P < 0.01$ and *, $P < 0.05$. All the results of ANOVAs and *t*-tests for the data presented in each figure are shown in Supplemental Data Set 2.

Accession Numbers

BRI1 (At4G39400), BSK1 (AT4G35230), PEPR1 (AT1G73080), AP2A1 (AT5G22770), AP1/2B1 (AT4G11380), AP2M (AT5G46630), and APP2S (AT1G47830).

Supplemental Data

Supplemental Figure 1. Cartoon and Surface Representation of The Putative Endocytic YXXΦ motifs in the BRI1 Kinase Domain.

Supplemental Figure 2. Multiple Sequence Alignment of the μ-homology Domain (MHD) of AP2M.

Supplemental Figure 3. The *in vitro* Kinase Activity of BRI1 Is Impaired by Substitution of the Tyrosine (Y) by Serine (S), Alanine (A) or Glutamic acid (E) in the Putative YXXΦ Motifs.

Supplemental Figure 4. Molecular Characterization of the *Arabidopsis* Transgenic Lines Harboring Y-to-F Mutations in the Putative YXXΦ Motifs in BRI1.

Supplemental Figure 5. Transgenic Lines Harboring Y-to-S Mutations at Y_{898} or Y_{956} in BRI1 Are Resistant to BRs and Exhibit Impaired BRI1 Internalization.

Supplemental Figure 6. Phosphorylation and Ubiquitination Profile of BRI1 Y-to-F Mutants

in vivo.

Supplemental Figure 7. Y-to-F Mutations in the Putative YXXΦ Motifs in BRI1 Do Not Affect BRI1 Recycling.

Supplemental Figure 8. The Vacuolar Targeting of BRI1 in the Transgenic Lines Harboring Y-to-F Mutations in Y_{898}, Y_{945}, Y_{956} and Y_{961} Residues is Impaired.

Supplemental Figure 9. Purification of GST-tagged AP2M-μ Homology Domain (MHD).

Supplemental Figure 10. BRI1 interacts directly with AP2A1 and AP2S *in vitro* in GST pull-down assays.

Supplemental Figure 11. Original Blots.

Supplemental Data Set 1. Primers Used in this Study.

Supplemental Data Set 2. Results of ANOVAs and *t*-tests for the Data Presented in Each Figure.

ACKNOWLEDGMENTS

We thank Steven C. Huber (University of Illinois Urbana-Champaign, Urbana, IL, USA) for discussions of the original project idea, Yanhai Yin (Iowa State University, Ames, IA, USA), Inhwan Hwang (Pohang University of Science and Technology, Pohang, Korea), Michael Hothorn (University of Geneva, Geneva, Switzerland), Christa Testerink (Wageningen University and Research, Wageningen, The Netherlands) and Ray Owens (University of Oxford, Oxford, United Kingdom) for providing the α-BES1 antibody, the α-AP2A antibody, the α-BRI1 antibody, and the pGEX KG and the pOPINJ plasmids respectively, and Martine De Cock for help in preparing the manuscript. The authors acknowledge the support and the use of resources of Instruct-ERIC (PID: 1724). This work was supported by grants from Ghent University Special Research Fund Grant (BOF 15/24J/048 to E.R.), the Austrian Science Fund/Research Foundation-Flanders joint project (FWF/FWO G0E5718N/I 3630-B25 to J.F. and E.R.), the Belgian Science Policy Office for a postdoctoral fellowship (R.K.), the China Scholarship Council for predoctoral fellowships (X.Z. and P.W.), the European Research Council (projects 682436 to D.V.D. and 742985 to J.F.), and Research Foundation-Flanders (FWO G009415N to D.V.D).

AUTHOR CONTRIBUTIONS

D.L., R.K. and E.R. designed the study; D.L. performed most of the experiments; R.K., I.V., L.A.N.C., W.S., X. Z. and P.W. performed experiments; A.J.J. and J.F contributed the

TIRFM; K.W.B., S.M., and G.V. performed experiments and contributed materials; K.Y. and D.V.D. contributed to the protein work; D.L. and E.R. wrote the manuscript. All authors revised the manuscript.

REFERENCES

Abas, L., Benjamins, R., Malenica, N., Paciorek, T., Wiśniewska, J., Moulinier-Anzola, J.C., Sieberer, T., Friml, J., and Luschnig, C. (2006). Intracellular trafficking and proteolysis of the Arabidopsis auxin-efflux facilitator PIN2 are involved in root gravitropism. Nat. Cell Biol. **8:** 249-256.

Adamowski, M., Narasimhan, M., Kania, U., Glanc, M., De Jaeger, G., and Friml, J. (2018). A functional study of AUXILIN-LIKE1 and 2, two putative clathrin uncoating factors in Arabidopsis. Plant Cell **30:** 700-716.

Asami, T., Min, Y.K., Nagata, N., Yamagishi, K., Takatsuto, S., Fujioka, S., Murofushi, N., Yamaguchi, I., and Yoshida, S. (2000). Characterization of brassinazole, a triazole-type brassinosteroid biosynthesis inhibitor. Plant Physiol. **123:** 93-99.

Bashline, L., Li, S., Anderson, C. T., Li, L., and Gu, Y. (2013). The endocytosis of cellulose synthase in Arabidopsis is dependent on μ2, a clathrin-mediated endocytosis adaptin. Plant Physiol. **163:** 150-160.

Bashline, L., Li, S., Zhu, X., and Gu, Y. (2015). The TWD40-2 protein and the AP2 complex cooperate in the clathrin-mediated endocytosis of cellulose synthase to regulate cellulose biosynthesis. Proc. Natl. Acad. Sci. USA **112:** 12870-12875.

Berrow, N. S., Alderton, D., Sainsbury, S., Nettleship, J., Assenberg, R., Rahman, N., Stuart, D.I., and Owens, R.J. (2007). A versatile ligation-independent cloning method suitable for high-throughput expression screening applications. Nucleic Acids Res. **35:** e45.

Böhm, S. K., Khitin, L.M., Smeekens, S.P., Grady, E.F, Payan, D.G., and Bunnett, N.W.(1997). Identification of potential tyrosine-containing endocytic motifs in the carboxyl-tail and seventh transmembrane domain of the neurokinin 1 receptor. J. Biol. Chem. **272:** 2363-2372.

Bojar, D., Martinez, J., Santiago, J., Rybin, V., Bayliss, R., and Hothorn, M. (2014). Crystal structures of the phosphorylated BRI1 kinase domain and implications for brassinosteroid signal initiation. Plant J. **78:** 31-43.

Bonifacino, J.S., and Traub, L.M. (2003). Signals for sorting of transmembrane proteins to endosomes and lysosomes. Annu. Rev. Biochem. **72:** 395-447.

Boruc, J., Van den Daele, H., Hollunder, J., Rombauts, S., Mylle, E., Hilson, P., Inzé, D., De Veylder, L., and Russinova, E. (2010). Functional modules in the *Arabidopsis* core cell cycle binary protein-protein interaction network. Plant Cell **22:** 1264-1280.

Clough, S.J., and Bent, A.F. (1998). Floral dip: A simplified method for Agrobacterium-mediated transformation of *Arabidopsis thaliana*. Plant J. 16: 735-743.

De Franceschi, N., Arjonen, A., Elkhatib, N., Denessiouk, K., Wrobel, A.G., Wilson, T.A., Pouwels, J., Montagnac, G., Owen, D.J., and Ivaska, J. (2016). Selective integrin endocytosis is driven by interactions between the integrin α-chain and AP2. Nat. Struct. Mol. Biol. **23:** 172-179.

Dhonukshe, P., Aniento, F., Hwang, I., Robinson, D.G., Mravec, J., Stierhof, Y.D., and Friml, J. (2007). Clathrin-mediated constitutive endocytosis of PIN auxin efflux carriers in *Arabidopsis*. Curr. Biol. **17:** 520-527.

Di Rubbo, S., Irani, N.G., Kim, S.Y., Xu, Z.Y., Gadeyne, A., Dejonghe, W., Vanhoutte, I., Persiau, G., Eeckhout, D., Simon, S., Song, K., Kleine-Vehn, J., Friml, J., De Jaeger, G., Van Damme, D., Hwang, I., and Russinova E. (2013). The clathrin adaptor complex AP-2 mediates endocytosis of BRASSINOSTEROID INSENSITIVE1 in *Arabidopsis*. Plant Cell **25:** 2986-2997.

Fan, L., Hao, H., Xue, Y., Zhang, L., Song, K., Ding, Z., Botella, M.A., Wang, H., and Lin, J. (2013). Dynamic analysis of *Arabidopsis* AP2 σ subunit reveals a key role in clathrin-mediated endocytosis and plant development. Development **140:** 3826-3837.

Fong, J. T., Kells, R. M., and Falk, M. M. (2013). Two tyrosine-based sorting signals in the Cx43 C-terminus cooperate to mediate gap junction endocytosis. Mol. Biol. Cell **24:** 2834-2848.

Fuji, K., Shirakawa. M., Shimono, Y., Kunieda, T., Fukao, Y., Koumoto, Y., Takahashi, H., Hara-Nishimura, I., and Shimada, T. (2016). The adaptor complex AP-4 regulates vacuolar protein sorting at the trans-Golgi network by interacting with VACUOLAR SORTING RECEPTOR1. Plant Physiol. **170:** 211-219.

Gadeyne, A., Sánchez-Rodríguez, C., Vanneste, S., Di Rubbo, S., Zauber, H., Vanneste, K., Van Leene, J., De Winne, N., Eeckhout, D., Persiau, G., Van De Slijke, E., Cannoot, B., Vercruysse, L., Mayers, J.R., Adamowski, M., Kania, U., Ehrlich, M., Schweighofer, A., Ketelaar, T., Maere, S., Bednarek, S.Y., Friml, J., Gevaert, K., Witters, E., Russinova, E., Persson, S., De Jaeger, G., and Van Damme, D. (2014). The TPLATE adaptor complex drives clathrin-mediated endocytosis in plants. Cell **156:** 691-704.

Geldner, N., Hyman, D. L., Wang, X., Schumacher, K., and Chory, J. (2007). Endosomal signaling of plant steroid receptor kinase BRI1. Genes Dev. **21:** 1598-1602.

Geldner, N., and Robatzek, S. (2008). Plant receptors go endosomal: a moving view on signal transduction. Plant Physiol. **147:** 1565-1574.

Gou, X., Yin, H., He, K., Du, J., Yi, J., Xu, S., Lin, H., Clouse, S.D., and Li, J. (2012). Genetic evidence for an indispensable role of somatic embryogenesis receptor kinases in brassinosteroid signaling. PLoS Genet. **8:** e1002452.

Grefen, C., and Blatt, M. R. (2012). A 2in1 cloning system enables ratiometric bimolecular fluorescence complementation (rBiFC). BioTechniques **53:** 311-314.

Gu, M., Schuske, K., Watanabe, S., Liu, Q., Baum, P., Garriga, G., and Jorgensen, E.M. (2008). μ2 adaptin facilitates but is not essential for synaptic vesicle recycling in *Caenorhabditis elegans*. J. Cell Biol. **183:** 881-892.

Hatsugai, N., Hillmer, R., Yamaoka, S., Hara-Nishimura, I., and Katagiri, F. (2016). The μ subunit of *Arabidopsis* adaptor protein-2 is involved in effector-triggered immunity mediated by membrane-localized resistance proteins. Mol. Plant-Microbe Interact. **29:** 345-351.

Huang, F., Jiang, X., and Sorkin, A. (2003). Tyrosine phosphorylation of the *β*2 subunit of clathrin adaptor complex AP-2 reveals the role of a di-leucine motif in the epidermal growth factor receptor trafficking. J. Biol. Chem. **278:** 43411-43417.

Huang, F., and Sorkin, A. (2005). Growth factor receptor binding protein 2-mediated recruitment of the RING domain of Cbl to the epidermal growth factor receptor is essential and sufficient to support receptor endocytosis. Mol. Biol. Cell **16:** 1268-1281.

Hunter, T. (2007). The age of crosstalk: Phosphorylation, ubiquitination, and beyond. Mol. Cell **28:** 730-738.

Hurley, J. H., Lee, S., and Prag, G. (2006). biquitin-binding domains. Biochem. J. **399:** 361-372.

Irani, N. G., Di Rubbo, S., Mylle, E., Van den Begin, J., Schneider-Pizoń, J., Hniliková, J., Šíša, M., Buyst, D., Vilarrasa-Blasi, J., Szatmári, A.M., Van Damme, D., Mishev,

K., Codreanu, M.C., Kohout, L., Strnad, M., Caño-Delgado, A.I., Friml, J., Madder, A., and Russinova, E. (2012). Fluorescent castasterone reveals BRI1 signaling from the plasma membrane. Nat. Chem. Biol. **8:** 583-589.

Jaillais, Y., Belkhadir, Y., Balsemão-Pires, E., Dangl, J. L., and Chory, J. (2011). Extracellular leucine-rich repeats as a platform for receptor/coreceptor complex formation. Proc. Natl. Acad. Sci. USA **108:** 8503-8507.

Johnson, A., and Vert, G. (2017). Single event resolution of plant plasma membrane protein endocytosis by TIRF microscopy. Front. Plant Sci. **8:** 612.

Karimi, M., Bleys, A., Vanderhaeghen, R., and Hilson, P. (2007). Building blocks for plant gene assembly. Plant Physiol. **145:** 1183-1191.

Kelly, B. T., McCoy, A.J., Späte, K., Miller, S.E., Evans, P.R., Höning, S., and Owen, D.J. (2008). A structural explanation for the binding of endocytic dileucine motifs by the AP2 complex. Nature **456:** 976-979.

Kim, S., Xu, Z., Song, K., Kim, D., Kang, H., Reichardt, I., Sohn, E.J., Friml, J., Juergens, G., and Hwang, I.(2013). Adaptor protein complex 2-mediated endocytosis is crucial for male reproductive organ development in *Arabidopsis*. Plant Cell **25:** 2970-2985.

Kitakura, S., Vanneste, S., Robert, S., Löfke, C., Teichmann, T., Tanaka, H., and Friml, J. (2011). Clathrin mediates endocytosis and polar distribution of PIN auxin transporters in *Arabidopsis*. Plant Cell **23:** 1920-1931.

Kleine-Vehn, J., Wabnik, K., Martinière, A., Łangowski, Ł., Willig, K., Naramoto, S., Leitner, J., Tanaka, H., Jakobs, S., Robert, S., Luschnig, C., Govaerts, W., Hell, S.W., Runions, J., and Friml, J. (2011). Recycling, clustering, and endocytosis jointly maintain PIN auxin carrier polarity at the plasma membrane. Mol. Syst. Biol. **7:** 540.

Konopka, C.A., Backues, S. K., and Bednarek, S. Y. (2008). Dynamics of Arabidopsis dynamin-related protein 1C and a clathrin light chain at the plasma membrane. Plant Cell **20:** 1363-1380.

Lamaze, C., and Schmid, S. L. (1995). Recruitment of epidermal growth factor receptors into coated pits requires their activated tyrosine kinase. J. Cell Biol. **129:** 47-54.

Lemmon, M. A., and Schlessinger, J. (2010). Cell signaling by receptor tyrosine kinases. Cell **141:** 1117-1134.

Li, X., and Pan, S. Q. (2017). *Agrobacterium* delivers VirE2 protein into host cells via clathrin-mediated endocytosis. Sci. Adv. **3:** e1601528.

Luo, Y., Scholl, S., Doering, A., Zhang, Y., Irani, N.G., Rubbo, S.D., Neumetzler, L., Krishnamoorthy, P., Van Houtte, I., Mylle, E., Bischoff, V., Vernhettes, S., Winne, J., Friml, J., Stierhof, Y.D., Schumacher, K., Persson, S., and Russinova, E. (2015). V-ATPase-activity in the TGN/EE is required for exocytosis and recycling in *Arabidopsis*. Nat. Plants **1:** 15094.

Luo, Y., and Russinova, E. (2017). Quantitative microscopic analysis of plasma membrane receptor dynamics in living plant cells. Methods Mol. Biol. **1564**: 121-132.

Ma, X., Claus, L.A.N., Leslie. M.E., Tao, K., Wu, Z., Liu, J., Yu, X., Li, B., Zhou, J., Savatin, D.V., Peng, J., Tyler, B.M., Heese, A., Russinova, E., He, P., and Shan, L. (2020). Ligand-induced BIK1 monoubiquitination regulates plant immunity. *Nature* in press (doi: 10.1038/s41586-020-2210-3).

Martins, S., Dohmann, E.M., Cayrel, A., Johnson, A., Fischer, W., Pojer, F., Satiat-Jeunemaître, B., Jaillais, Y., Chory, J., Geldner, N., and Vert, G. (2015). Internalization and vacuolar targeting of the brassinosteroid hormone receptor BRI1 are regulated by ubiquitination. Nat. Commun. **6:** 6151.

Mitsunari, T., Nakatsu, F., Shioda, N., Love, P.E., Grinberg, A., Bonifacino, J.S., and Ohno, H. (2005). Clathrin adaptor AP-2 is essential for early embryonal development. Mol. Cell. Biol. **25:** 9318-9323.

Mosesso, N., Bläske, T., Nagel, M.-K., Laumann, M., and Isono, E. (2018). Preparation of clathrin-coated vesicles from *Arabidopsis thaliana* seedlings. Front. Plant Sci. **9:** 1972.

Motley, A., Bright, N. A., Seaman, M. N. J., and Robinson, M. S. (2003). Clathrin-mediated endocytosis in AP-2--depleted cells. J. Cell Biol. **162:** 909-918.

Moulinier-Anzola, J., Schwihla, M., De-Araújo, L., Artner, C., Jörg, L., Konstantinova, N., Luschnig, C., and Korbei, B. (2020). TOLs function as ubiquitin receptors in the early steps of the ESCRT pathway in higher plants. *Mol. Plant*, in press (doi: 10.1016/j.molp.2020.02.012).

Nagel, M.K., Kalinowska, K., Vogel, K., Reynolds, G.D., Wu, Z., Anzenberger, F., Ichikawa, M., Tsutsumi, C., Sato, M.H., Kuster, B., Bednarek, S.Y., and Isono, E. (2017). *Arabidopsis* SH3P2 is an ubiquitin-binding protein that functions together with ESCRT-I and the deubiquitylating enzyme AMSH3. Proc. Natl. Acad. Sci. USA **114:** E7197-E7204.

Narasimhan, M., Johnson, A., Prizak, R., Kaufmann, W.A., Tan, S., Casillas-Pérez, B., and Friml, J. (2020). Evolutionarily unique mechanistic framework of clathrin-mediated endocytosis in plants. eLife **9:** e52067.

Nesterov, A., Carter, R. E., Sorkina, T., Gill, G. N., and Sorkin, A. (1999). Inhibition of the receptor-binding function of clathrin adaptor protein AP-2 by dominant-negative mutant μ2 subunit and its effects on endocytosis. EMBO J. **18:** 2489-2499.

Nolan, T., Vukašinović, N., Liu, D., Russinova, E., and Yin, Y. (2020). Brassinosteroids: Multi-dimensional regulators of plant growth, development, and stress responses. Plant Cell **32:** 295-318.

Ogiso, H., Ishitani, R., Nureki, O., Fukai, S., Yamanaka, M., Kim, J.H., Saito, K., Sakamoto, A., Inoue, M., Shirouzu, M., and Yokoyama, S. (2002). Crystal structure of the complex of human epidermal growth factor and receptor extracellular domains. Cell **110:** 775-787.

Oh, M.-H., Wang, X., Kota, U., Goshe, M.B., Clouse, S.D., and Huber, S.C. (2009a). Tyrosine phosphorylation of the BRI1 receptor kinase emerges as a component of brassinosteroid signaling in *Arabidopsis*. Proc. Natl. Acad. Sci. USA **106:** 658-663.

Oh, M.-H., Clouse, S. D., and Huber, S. C. (2009b). Tyrosine phosphorylation in brassinosteroid signaling. Plant Signal. Behav. **4:** 1182-1185.

Ohno, H., Stewart, J., **Fournier, M.C.,** Bosshart, **H., Rhee, I., Miyatake, S., Saito, T., Gallusser, A., Kirchhausen, T., and Bonifacino, J.S.** (1995). Interaction of tyrosine-based sorting signals with clathrin-associated proteins. Science **269:** 1872-1875.

Ortiz-Morea, F. A., Savatin, D.V., Dejonghe, W., Kumar, R., Luo, Y., Adamowski, M., Van den Begin, J. Dressano, K., Pereira de Oliveira, G., Zhao, X., Lu, Q., Madder, A., Friml, J., Scherer de Moura, D., and Russinova, E. (2016). Danger-associated peptide signaling in *Arabidopsis* requires clathrin. Proc. Natl. Acad. Sci. USA **113:** 11028-11033.

Owen, D. J., and Evans, P. R. (1998). A structural explanation for the recognition of tyrosine-based endocytotic signals. Science **282:** 1327-1332.

P**ettersen, E. F., Goddard, T.D., Huang, C.C., Couch, G.S., Greenblatt, D.M., Meng, E.C., and Ferrin, T.E.** (2004). UCSF Chimera-A visualization system for exploratory research and analysis. J. Comput. Chem. **25:** 1605-1612.

Reynolds, G. D., Wang, C., Pan, J., and Bednarek, S. Y. (2018). Inroads into internalization: five years of endocytic exploration. Plant Physiol. **176:** 208-218.

Ron, M., and Avni, A. (2004). The receptor for the fungal elicitor ethylene-inducing xylanase is a member of a resistance-like gene family in tomato. Plant Cell **16:** 1604-1615.

Russinova, E., Borst, J.W., Kwaaitaal, M., Caño-Delgado, A., Yin, Y., Chory, J., and de Vries, S.C. (2004). Heterodimerization and endocytosis of Arabidopsis brassinosteroid receptors BRI1 and AtSERK3 (BAK1). Plant Cell **16:** 3216-3229.

Sancho-Andrés, G., Soriano-Ortega, E., Gao, C., Bernabé-Orts, J.M., Narasimhan, M., Müller, A.O., Tejos, R., Jiang, L., Friml, J., Aniento, F., and Marcote, M.J. (2016). Sorting motifs involved in the trafficking and localization of the PIN1 auxin efflux carrier. Plant Physiol. **171:** 1965-1982.

Sorkin, A., and Carpenter, G. (1993). Interaction of activated EGF receptors with coated pit adaptins. Science **261:** 612-615.

Takano, J., Tanaka, M., Toyoda, A., Miwa, K., Kasai, K., Fuji, K., Onouchi, H., Naito, S., and Fujiwara, T. (2010). Polar localization and degradation of *Arabidopsis* boron transporters through distinct trafficking pathways. Proc. Natl. Acad. Sci. USA **107:** 5220-5225.

Tang, W., Kim, T.W., Oses-Prieto, J.A., Sun, Y., Deng, Z., Zhu, S., Wang, R., Burlingame, A.L., and Wang, Z.Y. (2008). BSKs mediate signal transduction from the receptor kinase BRI1 in *Arabidopsis*. Science **321:** 557-560.

Traub, L. M., and Bonifacino, J. S. (2013). Cargo recognition in clathrin-mediated endocytosis. Cold Spring Harb. Perspect. Biol. **5:** a016790.

Wang, C., Yan, X., Chen, Q., Jiang, N., Fu, W., Ma, B., Liu, J., Li, C., Bednarek, S.Y., and Pan, J. (2013). Clathrin light chains regulate clathrin-mediated trafficking, auxin signaling, and development in *Arabidopsis*. Plant Cell **25:** 499-516.

Wang, S., Yoshinari, A., Shimada, T., Hara-Nishimura, I., Mitani-Ueno, N., Ma, J., Naito, S., and Takano, J. (2017). Polar localization of the NIP5;1 boric acid channel is maintained by endocytosis and facilitates boron transport in Arabidopsis roots. Plant Cell **29:** 824-842.

Wang, X., Kota, U., He, K., Blackburn, K., Li, J., Goshe, M.B., Huber, S.C., and Clouse, S.D. (2008). Sequential transphosphorylation of the BRI1/BAK1 receptor kinase complex impacts early events in brassinosteroid signaling. Dev. Cell **15:** 220-235.

Wang, X., Goshe, M.B., Soderblom, E.J., Phinney, B.S., Kuchar, J.A., Li, J., Asami, T., Yoshida, S., Huber, S.C., and Clouse, S.D. (2005). Identification and functional analysis of in vivo phosphorylation sites of the *Arabidopsis* brassinosteroid-insensitive1 receptor kinase. Plant Cell **17:** 1685-1703.

Weinberg, J., and Drubin, D. G. (2012). Clathrin-mediated endocytosis in budding yeast. Trends Cell Biol. **22:** 1-13.

Yamamoto, M., Nishio, T., and Nasrallah, J. B. (2018). Activation of self-incompatibility signaling in transgenic *Arabidopsis thaliana* is independent of AP2-based clathrin-mediated endocytosis. G3 (Bethesda) **8:** 2231-2239.

Yamaoka, S., Shimono, Y., Shirakawa, M., Fukao, Y., Kawase, T., Hatsugai, N., Tamura, K., Shimada, T., and Hara-Nishimura, I. (2013). Identification and dynamics of *Arabidopsis* adaptor protein-2 complex and its involvement in floral organ development. Plant Cell **25:** 2958-2969.

Yin, Y., Wang, Z., Mora-Garcia, S., Li, J., Yoshida, S., Asami, T., and Chory, J. (2002). BES1 accumulates in the nucleus in response to brassinosteroids to regulate gene expression and promote stem elongation. Cell **109:** 181-191.

Yoshinari, A., Hosokawa, T., Amano, T., Beier, M.P., Kunieda, T., Shimada, T., Hara-Nishimura, I., Naito, S., and Takano, J. (2019). Polar localization of the borate exporter BOR1 requires AP2-dependent endocytosis. Plant Physiol. **179**: 1569-1580.

Yoshinari, A., Kasai, K., Fujiwara, T., Naito, S., and Takano, J. (2012). Polar localization and endocytic degradation of a boron transporter, BOR1, is dependent on specific tyrosine residues. Plant Signal. Behav. **7:** 46-49.

Zhou, J., Liu, D., Wang, P., Ma, X., Lin, W., Chen, S., Mishev, K., Lu, D., Kumar, R., Vanhoutte, I., Meng, X., He, P., Russinova, E., and Shan, L. (2018). Regulation of *Arabidopsis* brassinosteroid receptor BRI1 endocytosis and degradation by plant U-box PUB12/PUB13-mediated ubiquitination. Proc. Natl. Acad. Sci. USA **115:** E1906-E1915.

Zizioli, D., Meyer, C., Guhde, G., Saftig, P., von Figura, K., and Schu, P. (1999). Early embryonic death of mice deficient in γ-adaptin. J. Biol. Chem. **274:** 5385-5390.

Zuo, J., Niu, Q.W., Nishizawa, N., Wu, Y., Kost, B., and Chua, N.H. (2000). KORRIGAN, an Arabidopsis endo-1,4-β-glucanase, localizes to the cell plate by polarized targeting and is essential for cytokinesis. Plant Cell **12:** 1137-1152.

Zwiewka, M., Feraru, E., Möller, B., Hwang, I., Feraru, M.I., Kleine-Vehn, J., Weijers, D., and Friml J. (2011). The AP-3 adaptor complex is required for vacuolar function in Arabidopsis. Cell Res. **21:** 1711-1722.

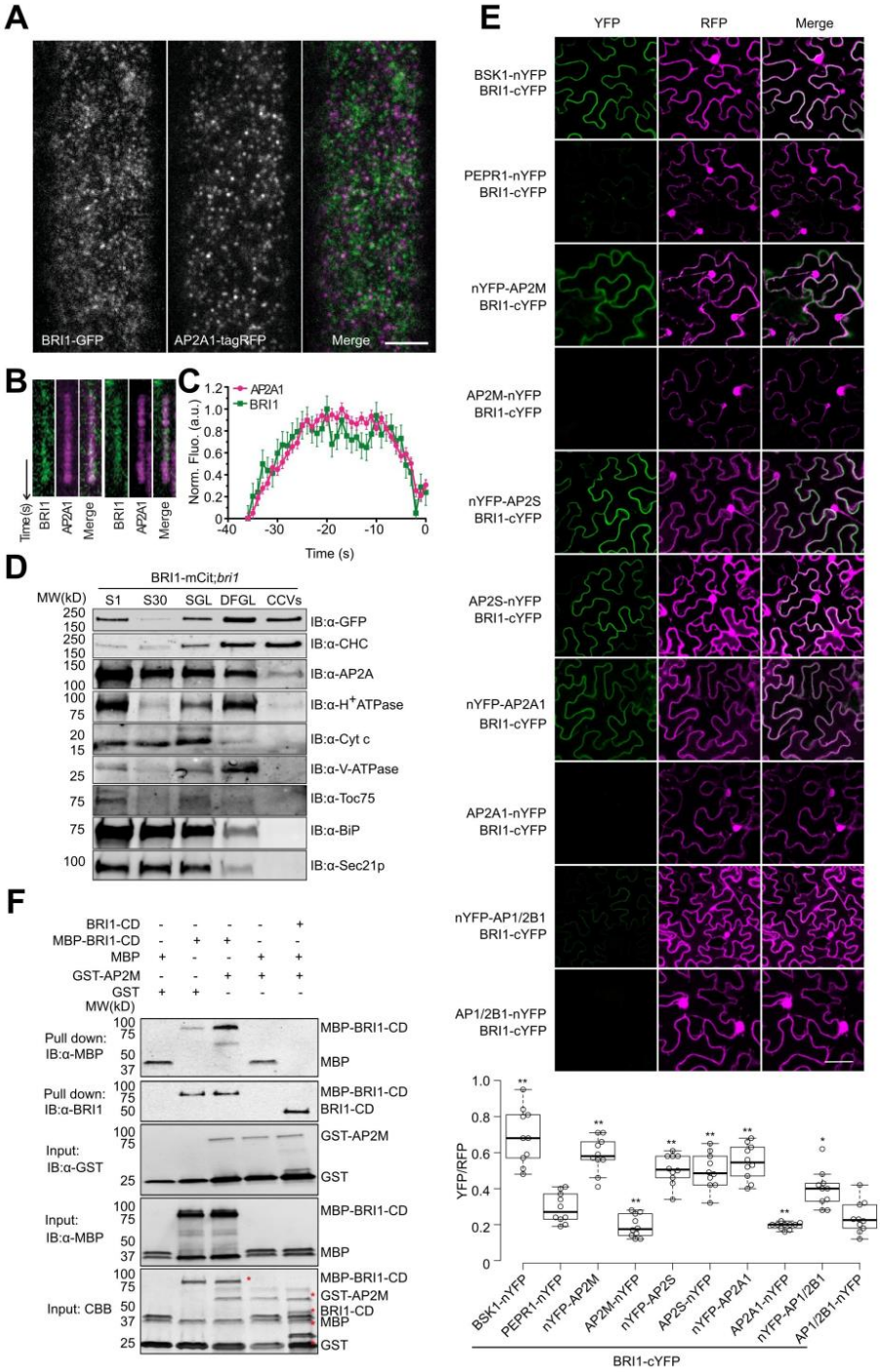

Figure 1. BRI1 Binds Directly to AP-2.
(A) TIRFM imaging of root epidermal cells of *Arabidopsis* BRI1-GFP;AP2A1-tagRFP;*bri1-116* plants. Scale bar, 5 μm.
(B) Kymographs of co-localizing foci.
(C) Departure assay plot of the normalized fluorescence of foci positive for both AP2A1 and BRI1 with the mean cell surface lifetime. Error bars indicate s.d. (*n* = 6, cells; *n* = 657, mean tracks; *n* = 6882, colocalized tracks).
(D) BRI1 fractionated with AP2A and clathrin in the CCV fraction. CCVs were prepared from total plant extracts of 7-day-old BRI1-mCitrine (mCit);*bri1* seedlings. Samples were collected during CCV purification and subjected to immunoblot (IB) analyses with antibodies against CHC, GFP, AP2A and various subcellular organelle marker proteins. S1, supernatant after centrifugation at 1,000×g; S30, supernatant after centrifugation at 30,000×g; SGL, sucrose step gradient load; CCV, CCV-containing fraction; DFGL, linear deuterium oxide/Ficoll gradient load. The following antibodies were used as organelle- or compartment-specific markers: α-H+ATPase (PM), α-Cyt c (mitochondria), α-V-ATPase (vacuole), α-TOC75 (chloroplast), α-BiP (endoplasmic reticulum), and α-SEC21p (COP-I vesicle).
(E) rBiFC analysis of BRI1 with different AP-2 subunits in *N. benthamiana* leaf epidermal cells. The combinations BSK1-nYFP/BRI1-cYFP and PEPR1-nYFP/BRI1-cYFP were used as positive and negative controls, respectively. Quantification of the ratio of the YFP fluorescence signal against RFP for different combinations is shown at the bottom. Box plots show the first and third quartiles, split by the medians (lines), with whiskers extending 1.5-fold interquartile range beyond the box. *n* = 10, cells. *P* values (one- way ANOVA and Tukey's post hoc), * <0.05; ** <0.01 relative to the PEPR1-nYFP/BRI1- cYFP control. Scale bar, 10 μm.
(F) BRI1 interaction with AP2M *in vitro*. Free MBP, MBP-fused BRI1-cytoplasmic domain (CD) (MBP-BRI1-CD), or MBP-BRI1-CD together with BRI1-CD was incubated with glutathione beads coupled with GST or GST-AP2M. The beads were collected and washed, followed by immunoblotting with α-MBP and α-BRI1. The protein inputs were determined by α-GST, α-MBP immunoblotting and Coomassie Brilliant Blue (CBB) staining. The positions of the corresponding proteins are labeled with red asterisks in the CBB panel.

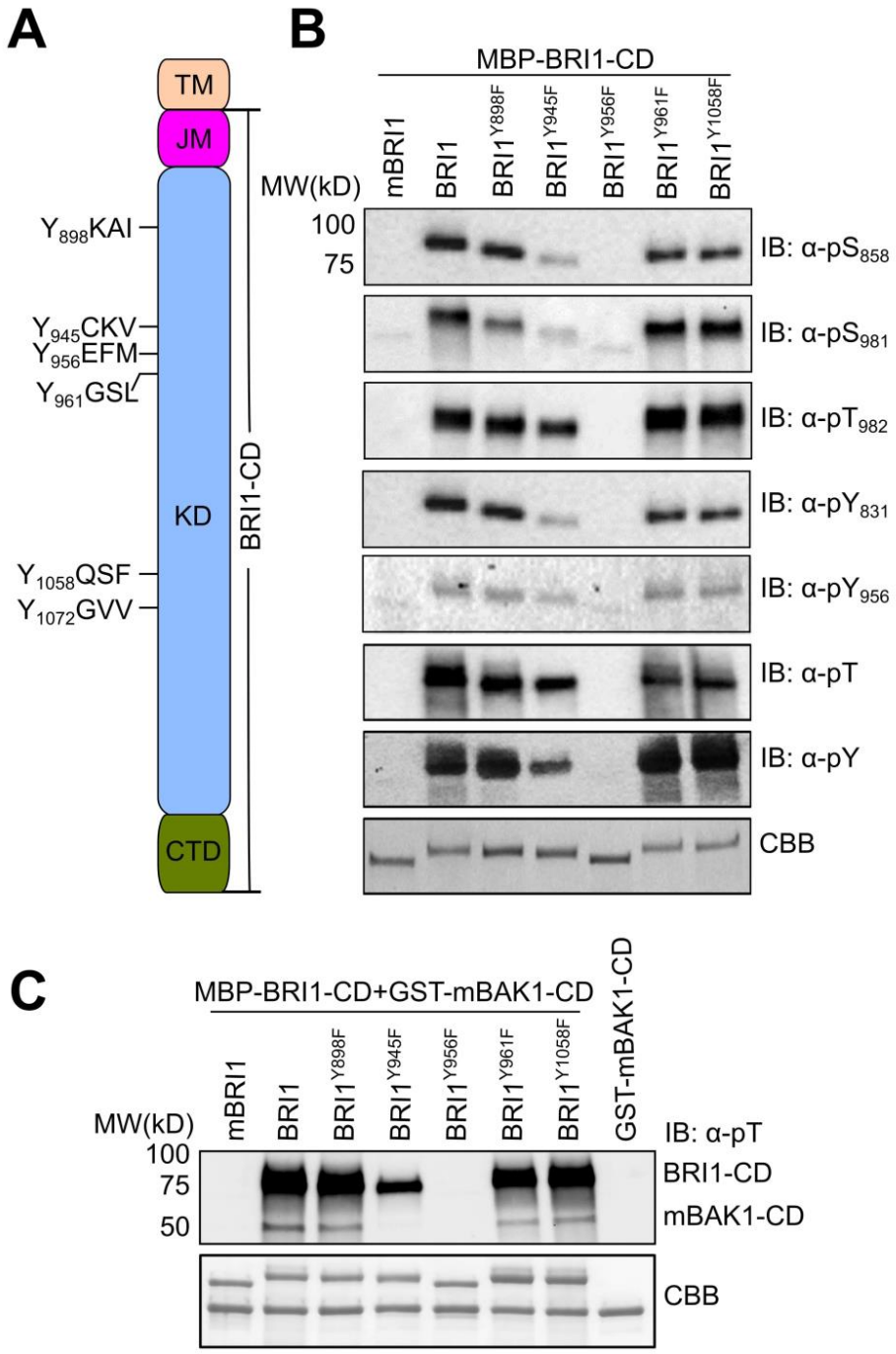

Figure 2. Identification of Putative Endocytic YXXΦ Motifs in BRI1.
(A) Schematic representation of the transmembrane and intercellular domains of BRI1 with the positions of the six canonical endocytic YXXΦ motifs. TM, transmembrane domain; JM, juxtamembrane domain; KD, kinase domain; CTD, C-terminal domain; CD, cytoplasmic domain.
(B) Effect of site-directed mutagenesis of tyrosine (Y) residues into phenylalanine (F) in BRI1- CD on autophosphorylation. Equal amounts of recombinant MBP-tagged wild type, Y- to-F mutated and inactive (BRI1K911E, mBRI1) recombinant BRI1-CD proteins were loaded and detected by immunoblotting (IB) with α-pS858, α-pS981, α-pT982, α-pY831, α-pY956, α-pT, and α-pY antibodies.
(C) Effect of site-directed mutagenesis of Y into F in BRI1-CD on the transphosphorylation of BAK1. Equal amounts of MBP-tagged wild type, Y-to-F mutated, and inactive (BRI1K911E, mBRI1) recombinant BRI1-CDs were combined with inactive GST-tagged BAK1 (BAK1D416N, mBAK1) CD in a kinase assay, followed by immunoblot detection with the α-pT antibody. Coomassie Brilliant Blue (CBB) staining was used as a loading control.

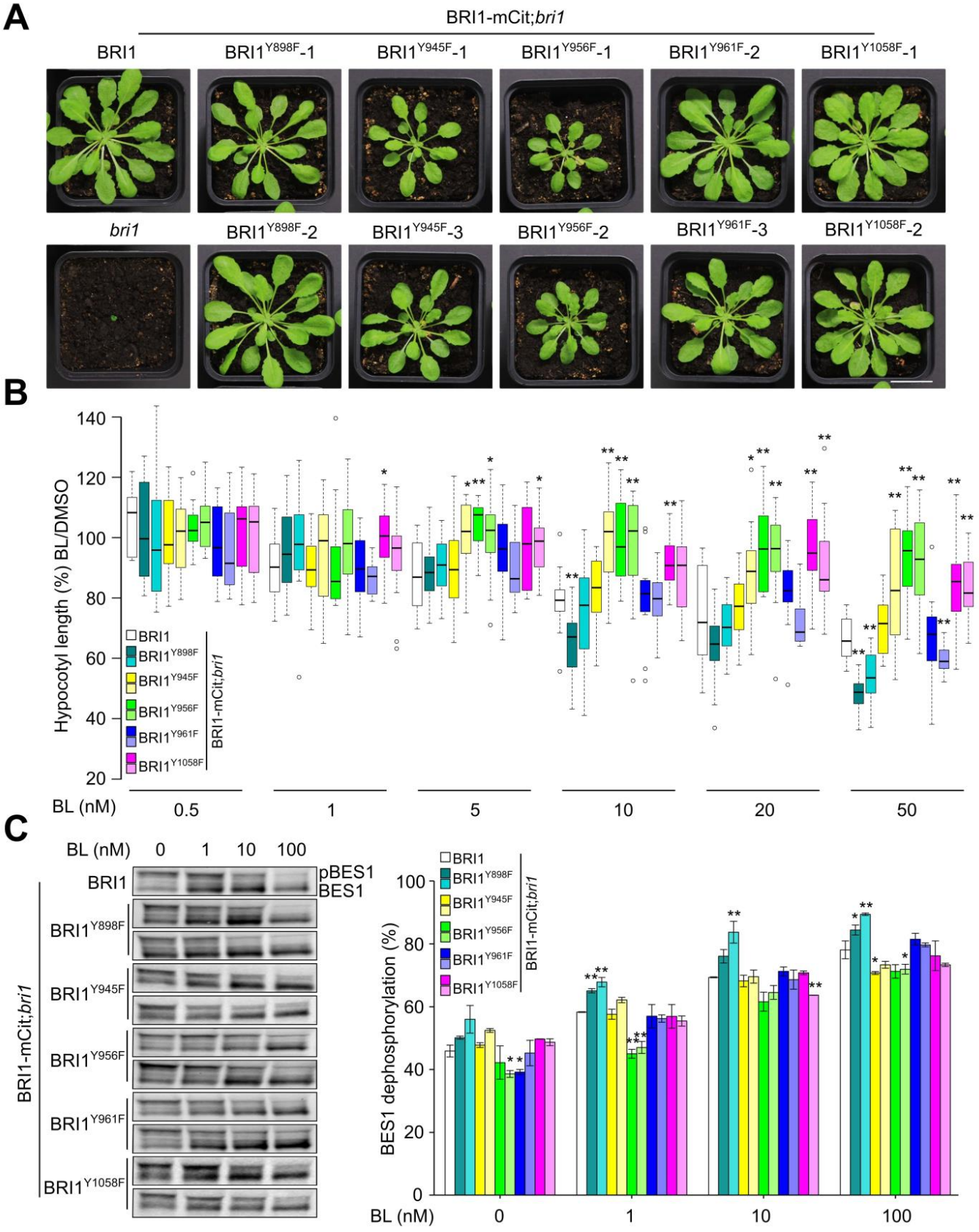

Figure 3. The BRI1Y898F Mutant Complements *bri1* and Causes BR Hypersensitivity.
(A) Growth phenotypes of 6-week-old soil-grown *Arabidopsis* plants. Two independent transgenic lines for each mutation are shown. Scale bar, 2 cm.
(B) Hypocotyl length (normalized to the DMSO control) of 5-day-old seedlings grown in the dark and in the presence of increasing concentrations of brassinolide (BL). For each transgenic line, at least 15 seedlings were measured. Box plots show the first and third quartiles, split by the medians (lines), with whiskers extending 1.5-fold interquartile range beyond the box. *P* values (one-way ANOVA and Tukey's post hoc) * <0.05; ** <0.01 relative to BRI1-mCitine (mCit);*bri1*.
(C) Total protein isolated from 5-day-old seedlings treated with increasing concentrations of BL for 1 h subjected to immunoblotting (IB) with α-BES1 to detect BES1 dephosphorylation. The percentage of dephosphorylated BES1 relative to the total BES1 from three independent experiments is shown on the right. Error bars indicate s.d. (*n* = 2, biological replicates [independent experiments]). *P* values (Student's *t*-test), * <0.05; ** <0.01 relative to BRI1mCit;*bri1*.

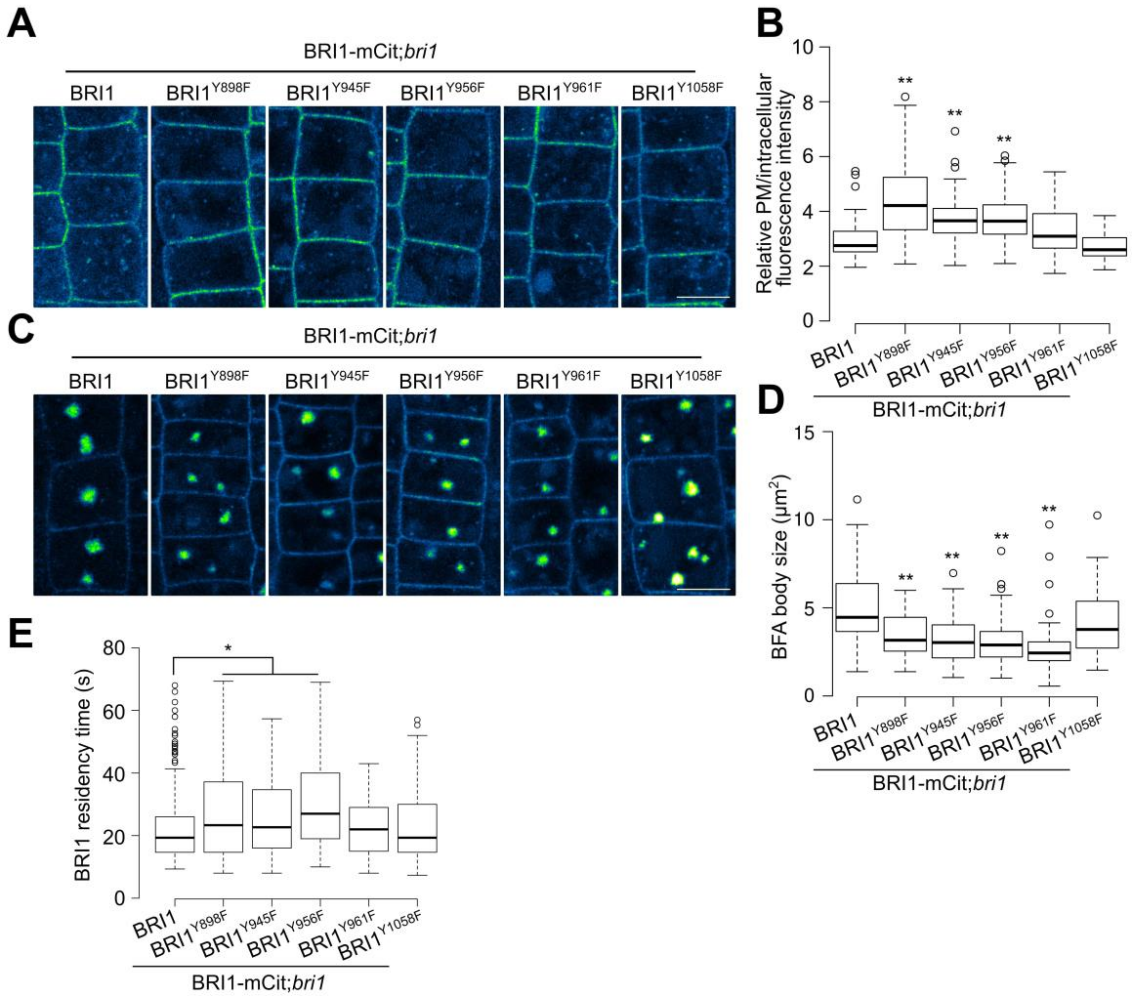

Figure 4. Y898F, Y945F, and Y956F Mutations Impair BRI1 Endocytosis.
(A) and **(C)** Images of epidermal cells from root meristems of 5-day-old transgenic *Arabidopsis* seedlings expressing different BRI1 mutants tagged with mCitrine (mCit) pre-treated with cycloheximide (CHX) (50 μM) for 1.5 h **(A)** or pre-treated with CHX (50 μM) for 1 h, followed by a combined treatment with CHX (50 μM) and Brefeldin A (BFA) (50 μM) for 30 min **(C)**. Green fire blue LUT in ImageJ was applied to the images to enhance contrast and highlight the differences between different transgenic lines. Scale bars, 5 μm.
(B) and **(D)** Measurements of the relative plasma membrane (PM) BRI1-mCit fluorescence and BFA body size. For each transgenic line, at least 50 cells from five seedlings were measured.
(E) Time of residency in the PM of BRI1-mCit. The box-plot was based on kymograph analysis of at least 100 tracks from 5 cells of at least three seedlings.
In **(B)**, **(D)**, and **(E)**, box plots show the first and third quartiles, split by the medians (lines), with whiskers extending 1.5-fold interquartile range beyond the box. *P* values (one-way ANOVA and Tukey's post hoc) * <0.05; ** <0.01 relative to BRI1-mCit;*bri1*.

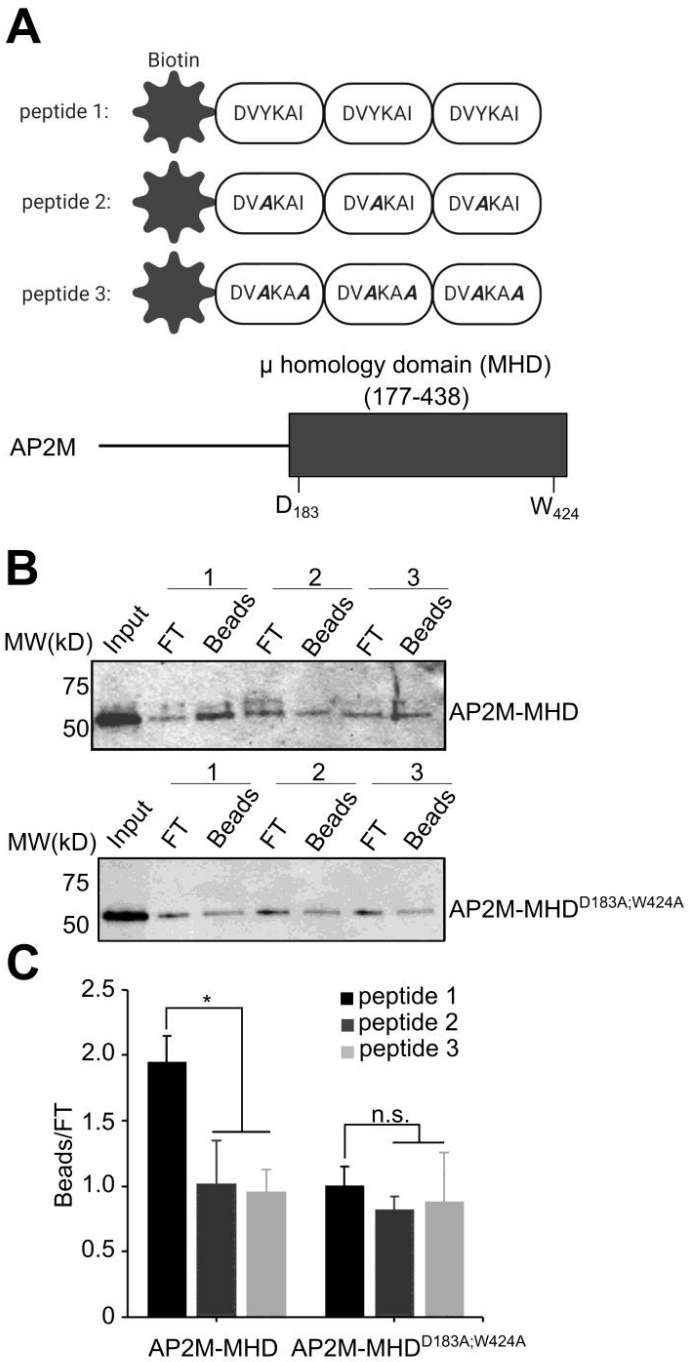

Figure 5. AP2M Binds to the Y898KAI Motif.
(A) Schematic representations of the N-terminally biotinylated peptides used for the *in vitro* peptide pull-down assay and the protein domain structure of *Arabidopsis* AP2M. MHD, the C-terminal μ homology domain of AP2M. The mutated residues are shown in bold italics, and the two residues (D183 and W424) in AP2M that are important for cargo recognition through the YXXΦ motif binding are indicated.
(B) Coupling of 200 ng of peptides to magnetic streptavidin beads, followed by incubation with purified GST-AP2M-MHD (top) or GST-AP2M-MHDD183A;W424A (bottom). The beads were collected and washed, followed by immunoblotting with α-GST. FT, Flow-through.
(C) Quantification of the interactions shown in **(B)**. Error bars indicate s.d. (n = 2, biological replicates [independent experiments]). P values (Student's t-test), * <0.05 relative to the peptide 1 pull-down control.

Endocytosis of BRASSINOSTEROID INSENSITIVE1 is Partly Driven by a Canonical Tyrosine-based Motif

Derui Liu, Rahul Kumar, Lucas A.N. Claus, Alexander Johnson, Wei Siao, Isabelle Vanhoutte, Peng Wang, Kyle W. Bender, Klaas Yperman, Sara Martins, Xiuyang Zhao, Grégory Vert, Daniel Van Damme, Jirí Friml and Eugenia Russinova

Plant Cell; originally published online September 21, 2020;
DOI 10.1105/tpc.20.00384